Aerodynamic Evaluation of Two Compact Radial Inflow Turbine Rotors

P. Susan Simonyi, Richard J. Roelke,
Roy G. Stabe, Brentley C. Nowlin,
and Danielle DiCicco

NASA
Technical
Paper
3514

1995

Aerodynamic Evaluation of Two Compact Radial Inflow Turbine Rotors

P. Susan Simonyi
Sverdrup Technology, Inc.
Lewis Research Center Group
Brook Park, Ohio

Richard J. Roelke
National Aeronautics and Space Administration
Lewis Research Center
Cleveland, Ohio

Roy G. Stabe
Sverdrup Technology, Inc.
Lewis Research Center Group
Brook Park, Ohio

Brentley C. Nowlin and Danielle DiCicco
National Aeronautics and Space Administration
Lewis Research Center
Cleveland, Ohio

Summary

The aerodynamic evaluation of two highly loaded compact radial turbine rotors was conducted at the NASA Lewis Research Center Small Engine Component Test Facility (SECTF). The experimental results were used for proof-of-concept, for modeling radial inflow turbine rotors, and for providing data for code verification.

Two rotors were designed to have a shorter axial length, up to a 10-percent reduced diameter, a lighter weight, and equal or higher efficiencies compared with those of conventional radial inflow turbine rotors. Three configurations were tested: rotor I, having a 40-percent shorter axial length, with the design stator (stator I); rotor I with the design stator vanes closed down (stator II); and rotor II, slightly shorter axially and having higher loading, with stator II. The stator had 36 vanes and the rotors each had 14 solid blades. Although presently uncooled, the rotor blades were designed for thicknesses which would allow cooling passages to be added.

The overall stage performance measurements and the rotor and stator exit flow field surveys were obtained. Measurements of steady state temperatures, pressures, mass flow rates, flow angles, and output power were made at various operating conditions. Data were obtained at corrected speeds of 80, 90, 100, 110, and 120 percent of design over a range of equivalent inlet-to-exit pressure ratios of 3.5, 4.0, 4.5, and 5.0, the maximum pressure ratio achieved.

The test showed that the configuration of rotor I with stator I running at the design pressure ratio produced a flow rate which was 5.6 percent higher than expected. This result indicated the need to close down the stator flow area to reduce the flow. The flow area reduction was accomplished by restaggering the vanes. Rotor I was retested with the closed-down stator vanes and achieved the correct mass flow. Rotor II was tested only with the restaggered vanes.

The test results of the three turbine configurations were nearly identical. Although the measured efficiencies of the compact designs fell 2 to 3 points below the predicted efficiency of 91 percent, they did meet and exceed by up to 2.5 percentage points the efficiencies of state-of-the-art turbines found in the literature.

Introduction

The performance of radial turbines can exceed that of axial turbines in small size applications. In addition, one radial stage may replace two or possibly more axial stages because of the higher stage pressure ratios that a radial turbine can achieve. The bulkiness and weight of radial inflow turbines, however, have made them difficult to incorporate in aircraft propulsion systems. To address this issue, a joint program was established between Pratt and Whitney Aircraft, the Army Propulsion Laboratory, and NASA Lewis Research Center to reduce the size (i.e., axial length) and weight of a radial inflow turbine rotor. Pratt and Whitney designed two highly loaded compact radial inflow turbine rotors, both parties analyzed the rotor flow fields with their respective design systems, and NASA Lewis conducted aerodynamic performance tests (refs. 1 to 4).

The design goals were to reduce the rotor axial length by 40 to 50 percent and the weight by 20 to 30 percent while maintaining or exceeding conventional state-of-the-art radial turbine efficiency. Carefully controlling the flow to avoid high losses in such a significantly shorter blade was aided by the use of a three-dimensional flow analysis code (ref. 1). Two compact radial turbine stages were designed using these computational tools and are representative of a rotorcraft main propulsion engine or a regional commuter aircraft application. The resulting turbine work factors ($gJ\Delta h/U_t^2$) of 1.1 to 1.2 and a pressure ratio of greater than 4.6 are indications of high aerodynamic loading.

All test and rig adapting hardware was provided by Pratt and Whitney. The blading was scaled up nominally 1.5 times the engine size to make it compatible with the Lewis Small Engine Component Test Facility. The turbine testing was conducted by Lewis personnel and the data shared by the two parties.

Three configurations were tested: rotor I with stator I; rotor I with stator II (stator I closed down to reduce the throat area); and rotor II with stator II only. The nozzle was restaggered after the first test showed a higher-than-design mass flow rate at the design stage pressure ratio.

Tests were conducted in warm air at an inlet total temperature of 860 R and over an inlet total pressure range of 45 to 50 psia. The test program consisted of measuring the overall stage performance and conducting radial and circumferential flow field surveys at various operating conditions at the turbine inlet and exit and in the vaneless space. The flow surveys measured fluid temperature, pressure, and flow angle. Measured performance results are compared with conventional radial inflow turbine performance found in the literature.

Symbols

D rotor diameter, in.

g conversion constant, 32.174 lb_m-ft/lb_f-sec^2

h specific work, Btu/lb_m

J conversion constant, 778 ft-lb_f/Btu

$\dot{m}$ mass flow, lb_m/sec

N rotor speed, rpm

P pressure, lb_f/in.^{2}

R_e Reynolds number, $m/\mu D_t$

T absolute temperature, R

U blade speed, ft/sec

V absolute velocity, ft/sec

VR velocity ratio, $[U_t/(2gJ\Delta h'_t)^{1/2}]$

W relative velocity, $(2gJ\Delta h')^{1/2}$, ft/sec

WF work factor, $gJ\Delta h'/U_t^2$

α absolute flow angle, deg

β relative flow angle, deg

γ ratio of specific heats

δ ratio of inlet total pressure to U.S. standard sea-level pressure, P'_1/P^*

ε specific-heat-ratio correction, $0.740/\{\gamma[2/(\gamma+1)]^{\gamma/(\gamma-1)}\}$

η efficiency

θ squared ratio of critical velocity at turbine inlet to critical velocity at U.S. standard sea-level temperature, $(V_{cr,1}/V^*_{cr})^2$

μ viscosity lb/sec-ft

τ torque, in.-lb

Subscripts:

bx axial length of the turbine blade

cr conditions at Mach 1.0

eq equivalent conditions

L based on torque

p pressure side

s suction side

t tip

0 station upstream of stator at inlet

1 station at stator leading edge

2 station at rotor inlet

3 station at rotor exit

4 station downstream of rotor (rotor exit survey plane)

Superscripts:

$'$ total state condition

$*$ U.S. standard sea-level conditions (temperature, 518.67 R; pressure, 4.696 lb_f/in.^{2})

Turbine Design and Research Hardware

The significant difference between this radial turbine design and that of a conventional radial turbine is the greatly shortened rotor axial length, achieved by shortening the exducer portion of the rotor blade and redistributing the blade aerodynamic loading forward. A three-dimensional, multiblade-row, Euler design code (ref. 1) was utilized to design the airfoil geometry. The final blade shapes were selected based on aerodynamic performance and rotor stress levels. Figure 1 compares the two compact rotors with a conventional baseline rotor having an equal power requirement. The length and diameter reductions specified for the compact rotors are relative to a number of high-work radial inflow turbines found in the literature (refs. 5 to 11). The comparison reveals a 40- to 52-percent reduction in axial length and a 4-percent reduction in diameter of the compact rotor relative to conventional turbines scaled to a 3119-hp requirement.

The single stator designed for both rotors has 36 constant-section stator vanes and is shown in figure 2. The vanes have transonic exit velocities. The two compact rotors are shown in the photographs of figure 3: rotor I (3(a)) and rotor II (3(b)). Both rotors had 14 blades with elliptical leading edges. The inducer portion of rotor I had radial elements whereas the leading edge of rotor II had a slight sweep to minimize a leading edge overspeed condition associated with the reduced tip speed.
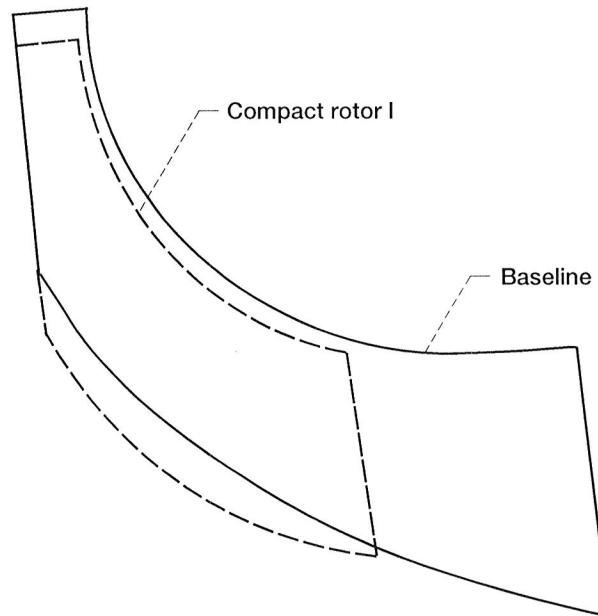
Figure 1.—Size comparison of compact rotors and baseline radial rotor.
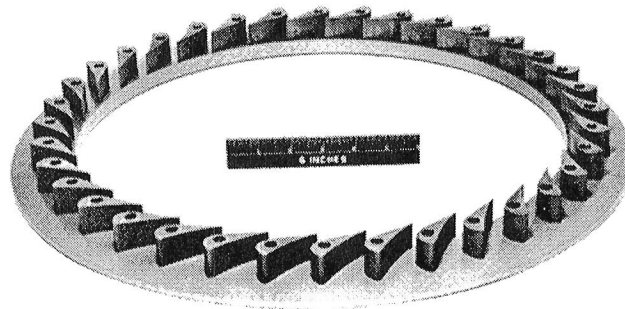
Figure 2.—Stator assembly.

The velocity diagrams for the two rotor configurations are shown in figure 4. As seen in 4(a), the stator has radial flow at the inlet and 73° of turning; rotor I has an incidence of 6.5° at the midspan and has a negative swirl at the exit. The velocity diagram in figure 4(b) is for the restaggered vane with rotor II. In this configuration, the vane turns the flow 71.5°; rotor II has an incidence of 21.4° and also has a negative exit swirl, which is a positive contribution toward turbine work output.

A comparison of the two compact rotors and the baseline rotor tested at the Lewis facility (ref. 5) is shown in figure 5. Although the stator and rotors tested were solid uncooled configurations, the aerodynamic contours were designed with sufficient thickness to accommodate internal cooling requirements.

Coordinates for the stator vanes, rotor blades, and endwalls for the test hardware are given in the tables and sketch of appendix A. The rotor blade geometry is listed for the hub and shroud and for three sections of the blade. Additional design details on the geometry are included in reference 2.

To utilize an existing research rig, the stator and rotors were scaled up from the design engine size. The stator and rotor I were

3

(a)

C-93-07728

C-93-07730

(b)

C-93-07729

C-93-07731
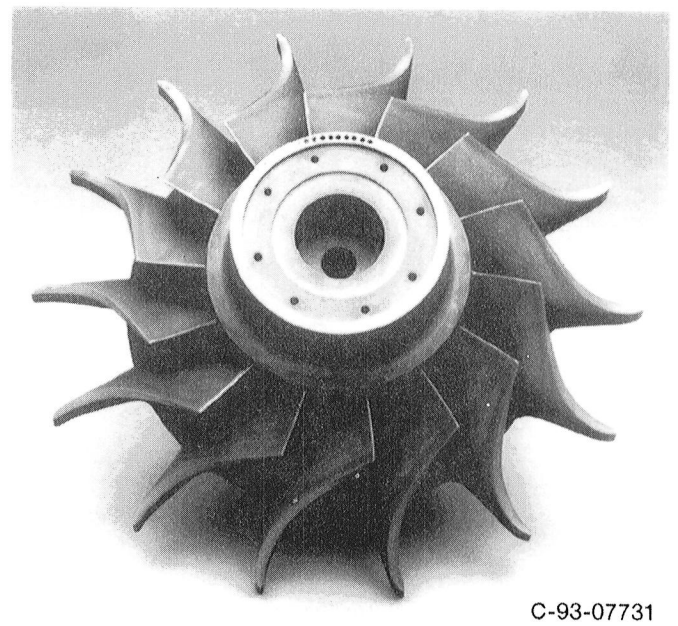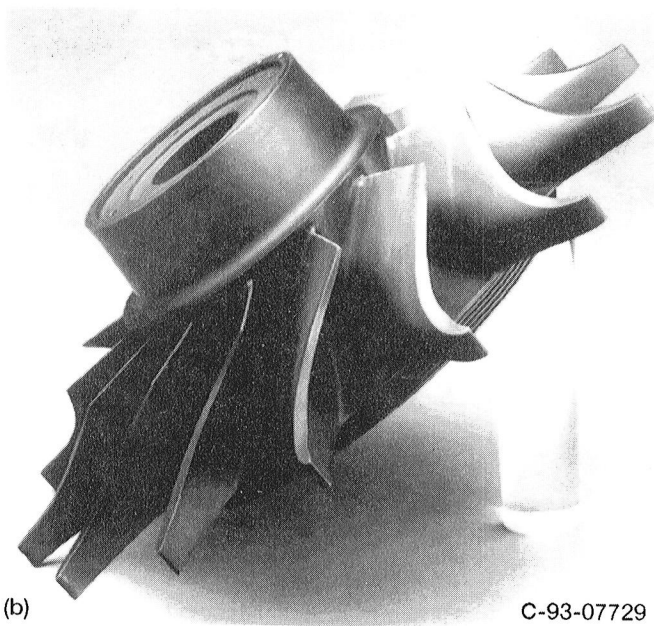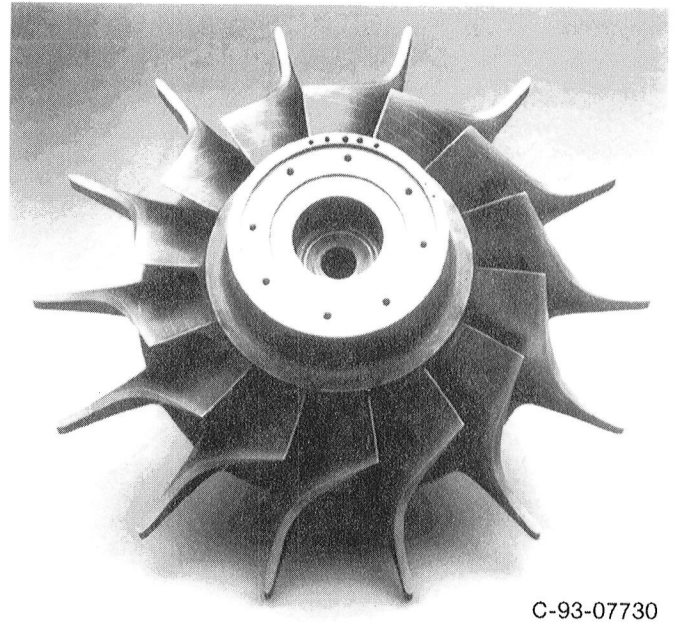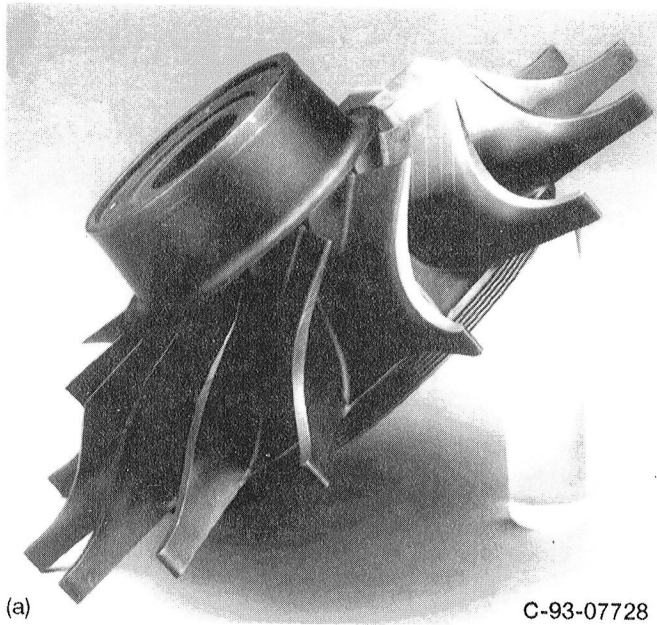
Figure 3.—Compact radial turbine rotors. (a) Test rotor I. (b) Test rotor II.
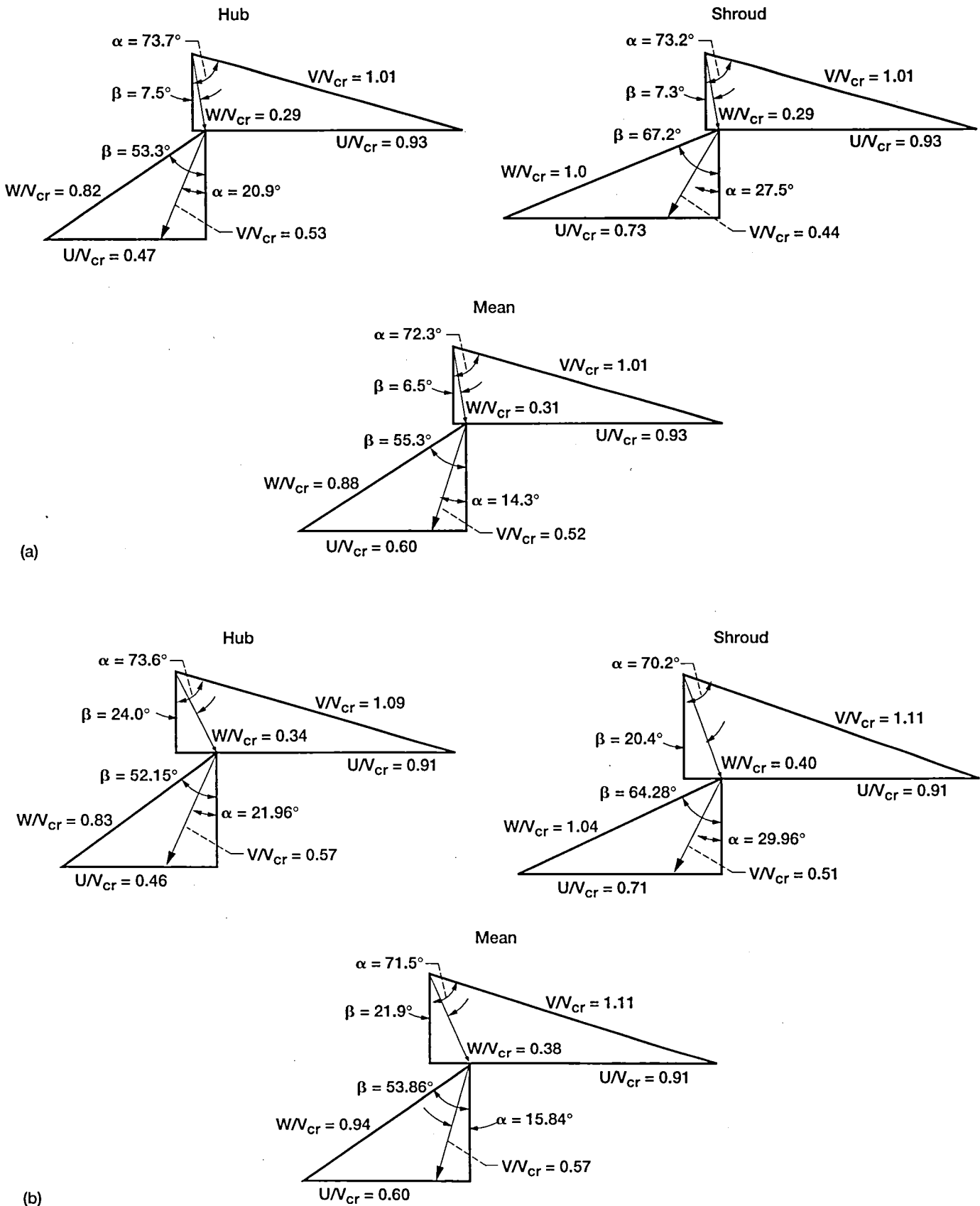
Figure 4.—Design velocity diagrams for two rotor configurations. (a) Rotor I with stator I. (b) Rotor II with stator II.
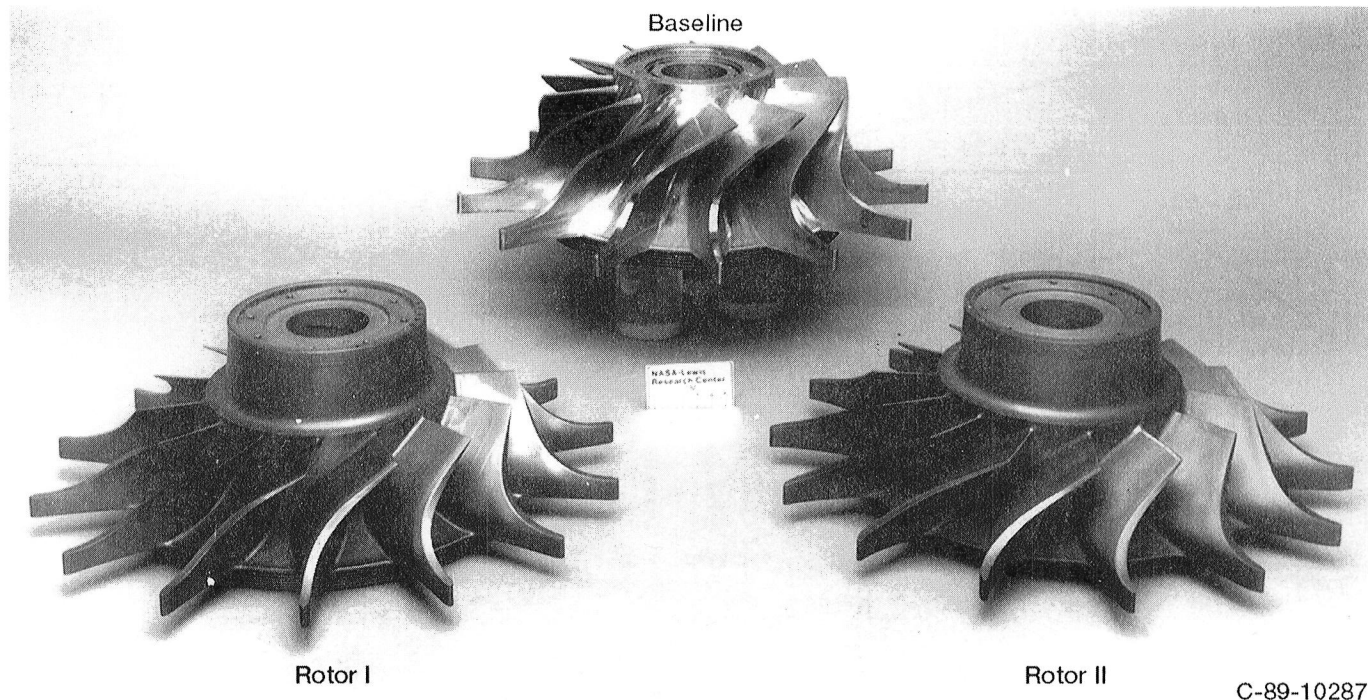
Figure 5.—Compact rotors compared with baseline rotor.

linearly scaled 1.503 times; rotor II was scaled 1.582 times to match the research rig. All aerodynamic and geometric parameters for the engine and test conditions were maintained similar.

Design parameters for the two compact radial turbines and for the engine and test hardware are listed in table I. Rotor I has a tip diameter of 9.62 in., a design mass flow of 9.57 lb_m/sec, a rotative speed of 54 596 rpm, and a work factor of 1.099. Rotor II has a tip diameter of 9.139 in., a design mass flow of 8.638 lb_m/sec, a rotative speed of 54 596 rpm, and a work factor of 1.218. After the rotors were scaled up to fit the rig, the rotors measured 14.59 in. in diameter. Both rotors were tested at an inlet total temperature of 860 R; rotor I was tested at a scaled design mass flow of 5.98 lb_m/sec and a rotative speed of 19 919 rpm. Rotor II was tested at a design mass flow of 5.622 lb_m/sec and a rotative speed of 18 923 rpm. Because the scale factor of rotor II had to be larger to fit the rig, the rotative speed had to be reduced to keep the similarity in the intended design velocity triangles.

The clearances between the rotor blades and the shroud were kept at a minimum: at the inducer portion of rotor I, it was 0.0207 in.; at the exducer, it was 0.0074 in. Rotor II had an inducer tip clearance of 0.0082 in. and an exducer tip clearance of 0.0146 in. The clearance in the backface region of the rotor was approximately 0.013 in. for both configurations. Of the three test configurations evaluated, the first consisted of the original stator and rotor I. The data from this test indicated an overflowing in the stator and an increased rotor reac-

tion. The stator was closed down 1.125° to more nearly match the design mass flow of 5.98 lb_m/sec. The restaggered nozzle was then used with compact rotors I and II to provide configurations two and three.

Apparatus, Instrumentation, and Procedure

These experiments were conducted in the Small Engine Components Test Facility at the NASA Lewis Research Center (ref. 6). Major components of the facility include the research turbine, the inlet and exhaust piping, a natural gas combustor, a torquemeter, a dynamometer, and the necessary controls, instrumentation, and data acquisition system. A schematic of the facility is shown in figure 6.

Air at 125 psig flows through the inlet control valve and into the natural gas combustor. The heated air then flows through an annular plenum, expands through the research turbine, and is exhausted to the altitude exhaust system, which can provide turbine exhaust pressures down to 2 psia. The mass flow rate is measured by a calibrated venturi.

Power produced by the research turbine is absorbed by an eddy current dynamometer which is also used to control the turbine speed. The rotational speed is measured by a magnetic pickup and a shaft-mounted gear. Torque is measured by an in-line, shaft-type torquemeter and is subsequently corrected

6

TABLE I.—AERODYNAMIC DESIGN PARAMETERS

Parameter	Rotor I		Rotor II	
	Engine	Test hardware	Engine	Test hardware
Total inlet temperature, T_0', R	2860	860	2860	860
Total inlet pressure, P_0', psia	319.1	48.4	319.1	45.5
Mass flow, $\dot{m}$ lb_m/sec	9.57	5.98	8.638	5.622
Equivalent mass flow, $\dot{m}_{eq}$, lb_m/sec	1.065	2.35	0.962	2.35
Rotor speed, N, rpm	54 596	19 919	54 596	18 923
Equivalent speed, N_{eq}, rpm	23 662	15 460	23 662	14 687
Specific work, h, BTU/lb_m	230.5	69.32	230.5	69.32
Equivalent specific work, h_{eq}, BTU/lb_m	43.29	41.75	43.29	41.75
Inlet-to-exit total pressure ratio, $P_0'P_3'$	4.627	4.992	4.627	4.992
Equivalent pressure ratio, $P_0'P_{3,eq}'$	3.5	4.88	3.5	4.88
Rotor tip diameter, D_t, in.	9.62	14.459	9.139	14.459
Blade tip speed, U_t, ft/sec	2292	1257	2177	1194
Velocity ratio, VR	0.674	0.674	0.641	0.641
Work factor, WF	1.099	1.099	1.218	1.1218
Reynolds number, $Re(bx, rel)$	643 000	642 500	568 250	568 780
Power, hp	3119	586	2815	551
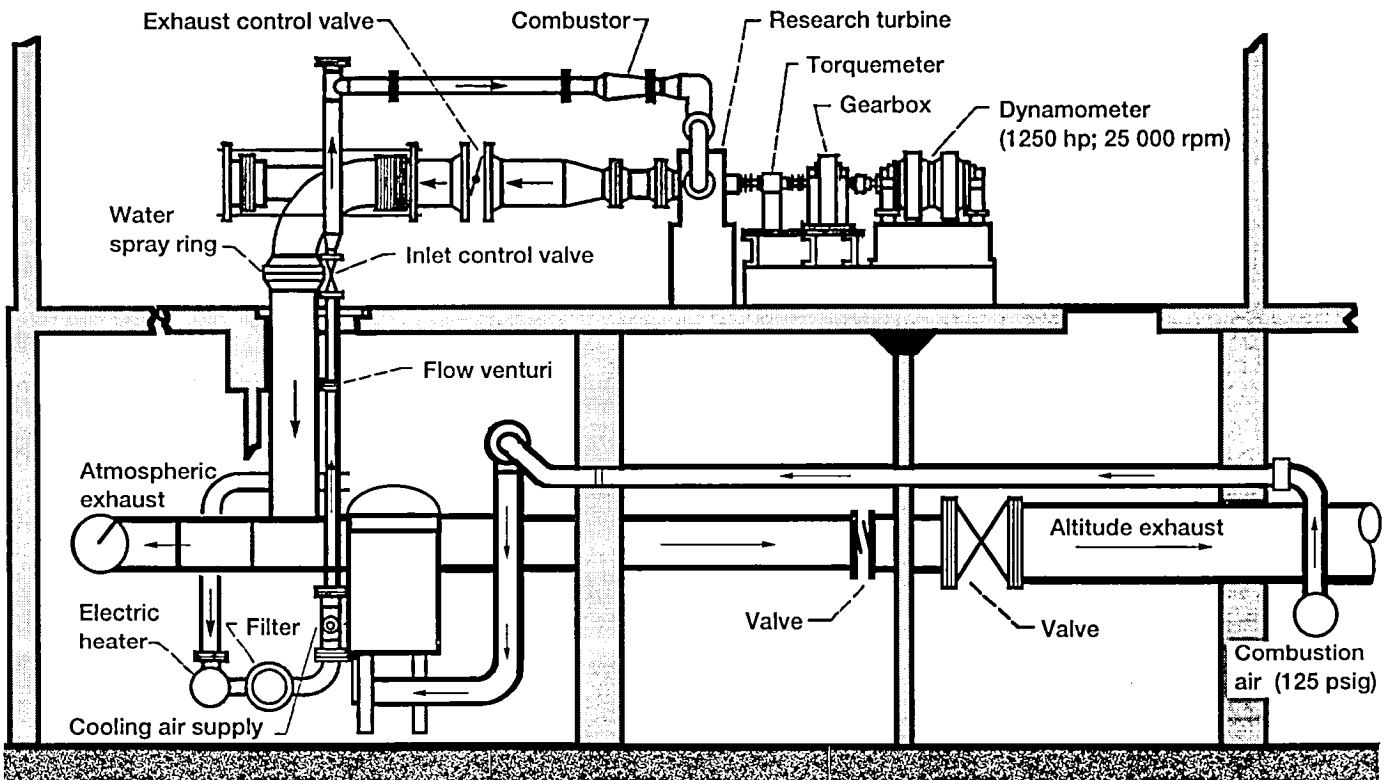
Figure 6.—Small engine components test facility (SECTF).
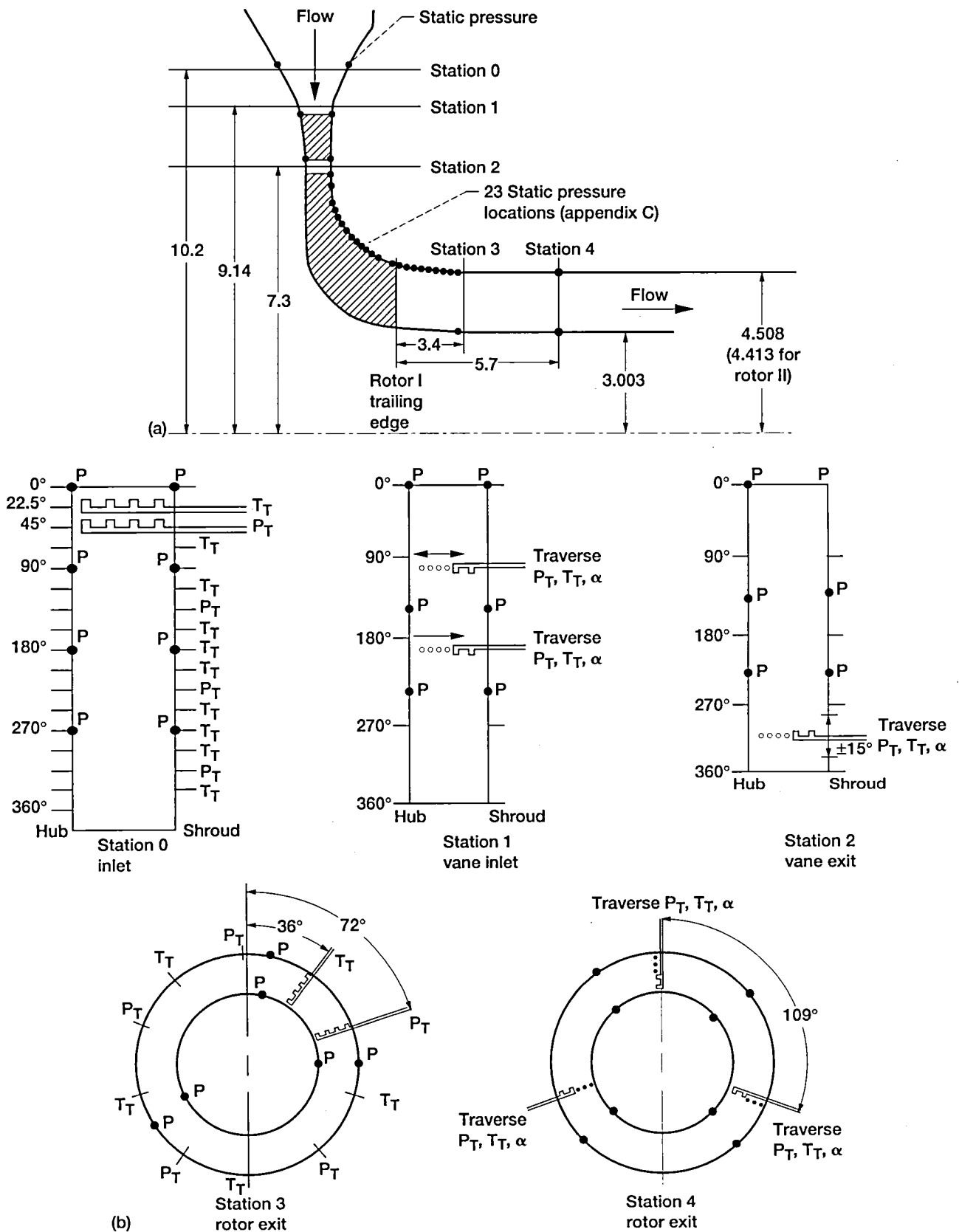
Figure 7.—Turbine test facility flow path instrumentation and measurement stations. (a) Instrumentation. (b) Measurement locations. All dimensions are in inches.

to reflect tare torque, which includes bearing, seal, and disk windage losses.

Figure 7 summarizes the turbine flow path instrumentation used during aerodynamic testing and identifies the measurement station locations. The turbine inlet total pressures and temperatures were measured using 14 fixed rakes at station 0, located at a radius of 10.2 in. from the rotor centerline. The turbine exit total pressures and temperatures were measured by using either 10 yaw adjustable rakes at station 3, located 3.4 in. downstream of the rotor trailing edge, or 3 radial traverse probes at station 4, located at 5.7 in. from the rotor trailing edge. Other instrumentation included a vane exit traverse probe, located midspan between the stator exit and the rotor inlet and used to obtain total temperature, pressure, and flow angle in the vaneless space (this probe traversed both the radial and circumferential directions). Clearance measurements and a number of static pressures were taken. A brief flow field survey at the stator inlet (station 1) was also made at the beginning of testing to confirm that the flow entering the stator was completely radial; this probe was removed for subsequent tests and the port plugged.

The overall performance and rotor exit survey tests were conducted for 80, 90, 100, 110, and 120 percent of design speed. At each speed, the inlet-to-exit pressure ratio was varied from 3.5 to 5.0, or to the maximum pressure ratio the test facility allowed. Exit rakes at station 3 were used to measure overall performance. Prior to a test, the turbine exit rakes were adjusted to a yaw angle defined by the predicted turbine exit swirl for that operating condition. After the turbine performance was measured using the fixed rakes at station 3, these rakes were removed and their endwall ports were plugged. Data were then acquired using station 4 radial traverse probes to measure detailed exit profiles of temperature, pressure, and air angle. Spanwise efficiencies were calculated and then mass-weighted to provide another measurement of turbine efficiency.

Results

Rotor I With Stator I

Figure 8 shows the measured mass flow as a function of the pressure ratio across the stage for various speed lines. The stage becomes choked for all the speed lines at various pressure ratios. For the 80- and 90-percent speed lines, the choked mass flow rate is approximately 2.48 lb_m/sec. The maximum mass flow rate decreases with increasing rotational speed, indicating that the rotor, rather than the stator, is choked. At the design pressure ratio of $P_0'/P_3' = 5.0$ and 100 percent of design speed, the measured mass flow was 5.6 percent above that intended.

Figure 9 shows the equivalent specific work as a function of the pressure ratio for the various speeds. At the design pres-
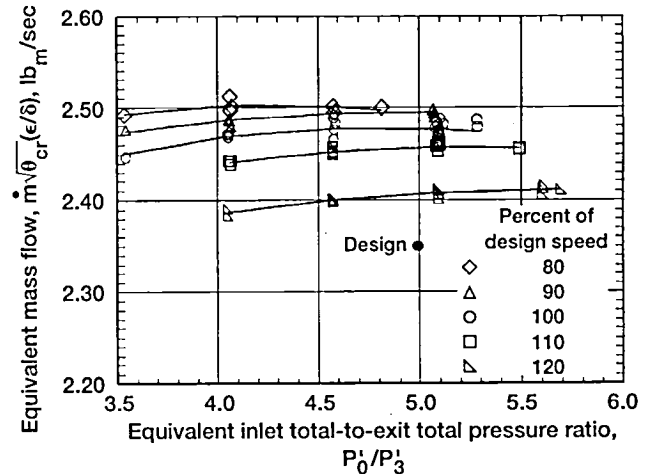
Figure 8.—Variation of mass flow rate with total-to-total pressure ratio for lines of constant speed for rotor I-stator I configuration.

sure ratio and speed, the measured specific work was 40 Btu/lb_m compared with the design intent of approximately 42 Btu/lb_m. At any pressure ratio, the maximum specific work occurred at 110 percent of the design speed.
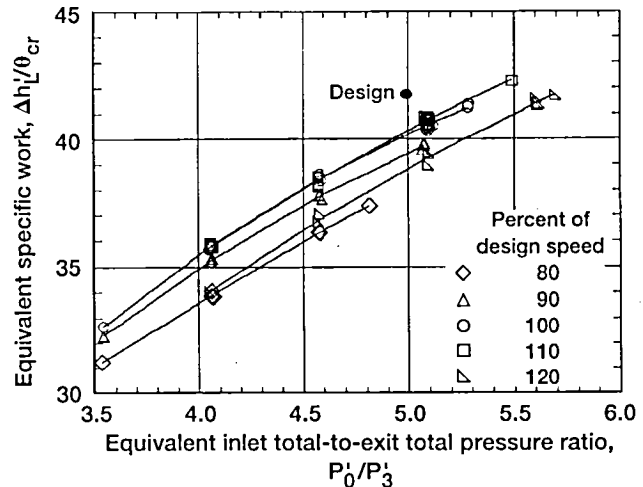
Figure 9.—Variation of specific work with total-to-total pressure ratio for lines of constant speed for rotor I-stator I configuration.

The equivalent torque for the various speed lines is presented in figure 10 as a function of the pressure ratio. The torque measured at the design pressure ratio and speed is 577 in.-lb. The turbine torque increases as the rotor speed drops with increasing pressure ratio. Limit loading has not occurred, as observed from figure 10 because an increasing pressure ratio still produces an increase in torque.

9
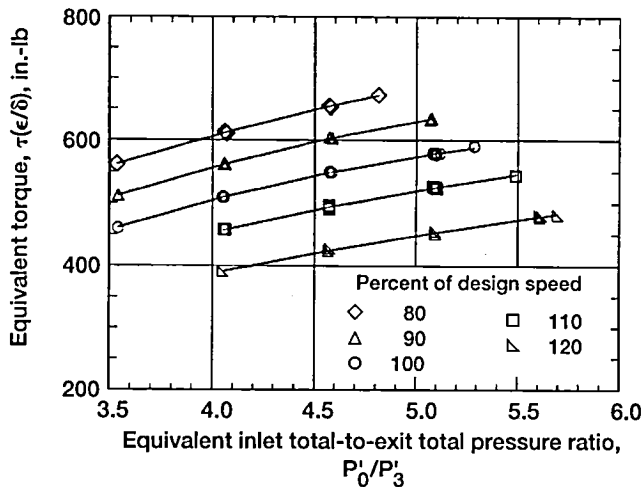
Figure 10.—Variation of turbine torque with total-to-total pressure ratio for lines of constant speed for rotor I-stator I configuration.

The turbine total efficiency is shown in figure 11(a) as a function of the pressure ratio. The total efficiency varied from 0.83 to 0.892 of the maximum total efficiency, which occurs at 110 percent speed. At the design pressure ratio and speed, the efficiency measured 0.884, which is 2.6 percent lower than the predicted value.

Figure 11(b) shows the total efficiency as a function of the work factor. Maximum efficiency is achieved at a work factor of 0.91 at 110 percent speed. At the design speed and pressure ratio, the work factor is 1.086 which is comparable to the design value of 1.099.

Rotor exit surveys were made using station 4 probes to measure the radial variation in temperature, total pressure, and flow angles. The rotor was operated over the same series of speeds and pressure ratios as previously discussed in the overall performance testing. The data presented in figures 12 to 15 for the exit surveys are at design conditions. At off-design speeds and pressure ratios, the flow characteristics were similar to those observed at design conditions. These results are presented in appendix B.

Figure 12 shows the flow angle data at station 4, downstream of the rotor. The exit flow angle varied radially from −18° near the hub to −30° at the midpoint and at the tip. The flow angles are measured with respect to blade rotation. A greater average swirl angle was measured than the design intent of −20°.

The ratio of exit total temperature to inlet total temperature as it varies from hub to tip at the rotor exit is shown in figure 13. The hub region has 2 percent lower temperatures than the tip region, which suggests that there is a slightly higher work extraction near the hub.

The ratio of inlet total to exit total pressure as it varies from hub to tip is presented in figure 14. The data show that there is a larger pressure drop in the tip area where unloading is occurring because of flow leakage through the tip region; however, the hub experiences less pressure drop.
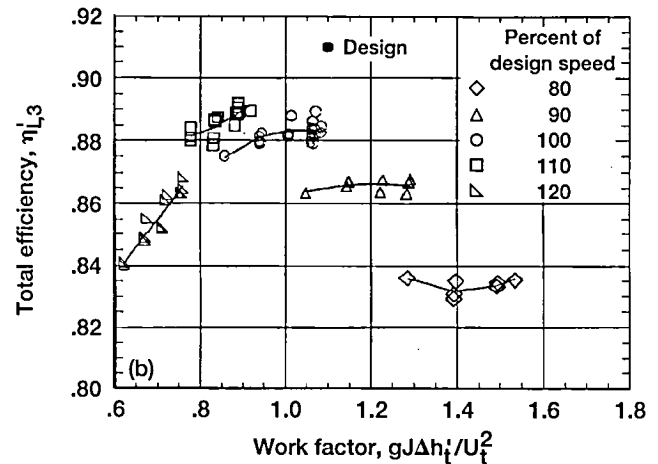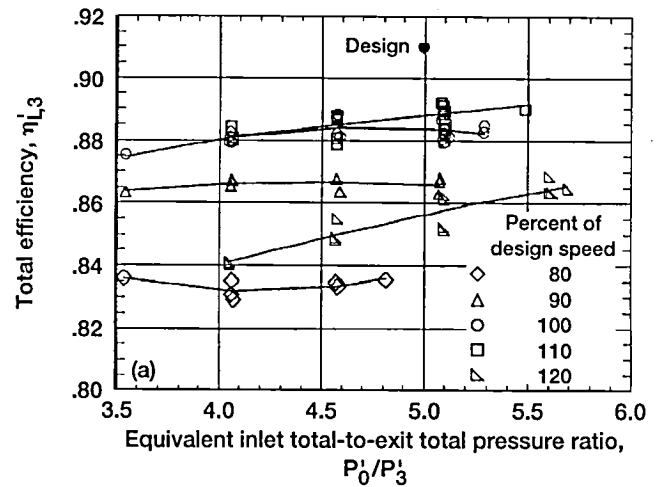
Figure 11.—Variation of total efficiency with total-to-total pressure ratio and work factor for lines of constant speed for rotor I-stator I configuration. (a) Total-to-total pressure ratio. (b) Work factor.
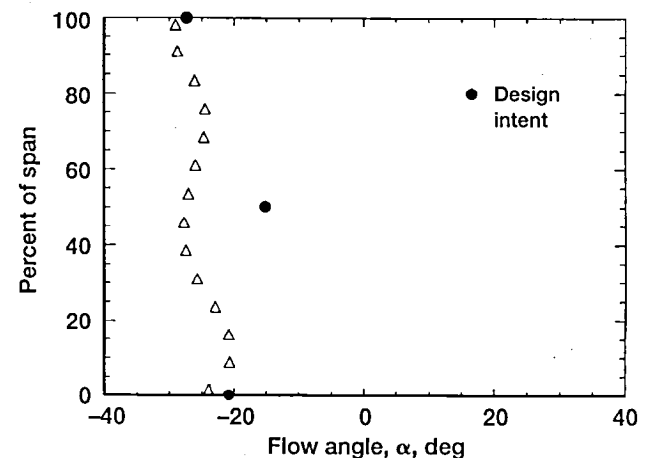
Figure 12.—Radial variation of exit flow angle at design operating condition for rotor I-stator I configuration.
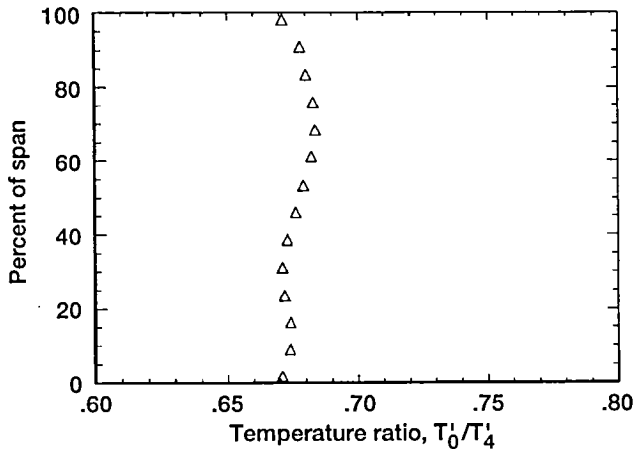
Figure 13.—Radial variation of exit-to-inlet total temperature ratio at design operating condition for rotor I-stator I configuration.
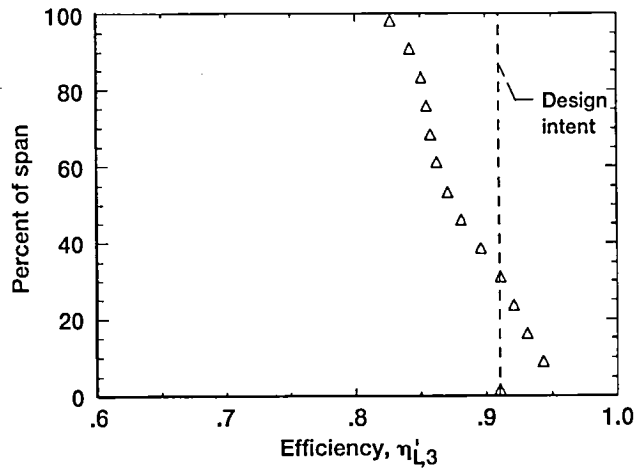
Figure 15.—Radial variation of total efficiency measured at rotor exit at design operating condition for rotor I-stator I configuration.
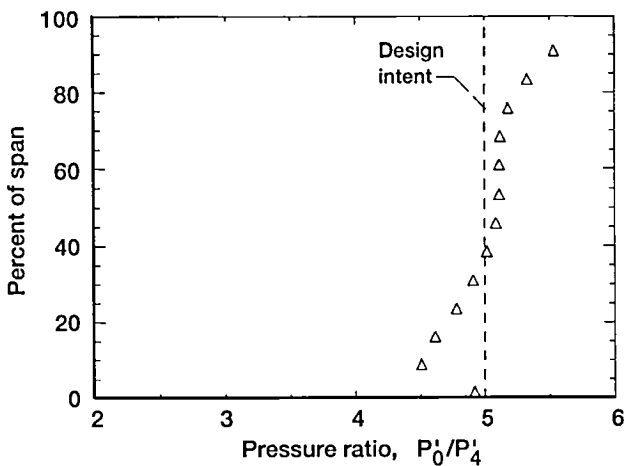
Figure 14.—Radial variation of exit-to-inlet total pressure ratio at design operating condition for rotor I-stator I configuration.
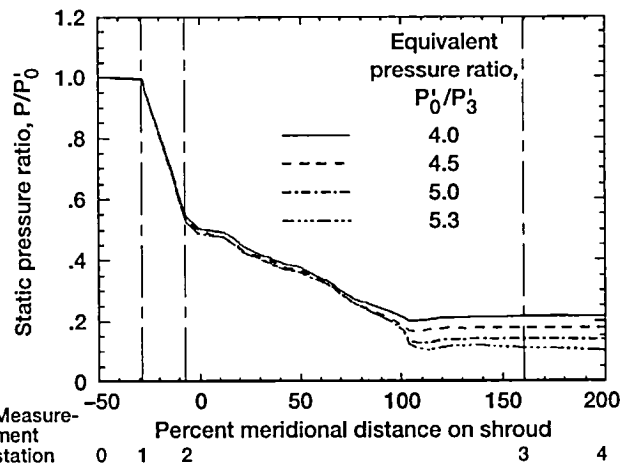
Figure 16.—Shroud static pressures over flow path for rotor I configuration.

Figure 15 shows the total efficiency, based on the temperature measurements taken by the survey instrumentation, as it varies at the exit of the rotor from hub to tip. There is almost a linear variation from hub to tip with a marked decrease right at the hub. As figures 13 and 14 suggest, the area near the hub is operating at a higher efficiency because of the larger work extraction and a lower pressure.

Static pressures were measured along the shroud of the turbine by several pressure taps located from the inlet of the stator (starting at the leading edge of the stator) and ending at

station 4. Appendix C gives the locations of these ports. The static pressure measured at the design speed for various pressure ratios is shown in figure 16. Static pressure decreased through the stator and the rotor at about the same rate. At the design pressure ratio, the amount of pressure drop in the stator was approximately 50 percent; another 50 percent of the pressure drop occurred in the rotor. Varying the inlet-to-exit pressure ratio caused the stator to have an approximately constant pressure drop because the rotor was choking. Figure 17 shows the static pressure variation over the rotor portion of the shroud.

11
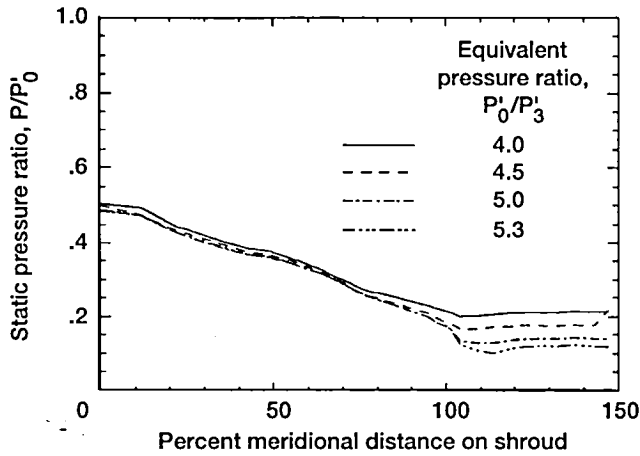
Figure 17.—Shroud static pressures over rotor I for various pressure ratios at design rotor speed.

Figure 18.—Exit survey results for closed-down stator II at design condition. (a) Circumferentially averaged flow angle at stator exit. (b) Circumferentially averaged spanwise variation of vane efficiency.

Stator II Exit Surveys

Because the first test configuration showed a 5.6 percent higher mass flow than the design intent, the stator area was closed down to obtain the correct design mass flow. After the stator vanes were restaggered by 1.125°, the stator exit flow was surveyed spanwise and circumferentially. Figures 18 and 19 show the survey results for the closed-down stator II at the design condition. Figure 18(a) shows the circumferentially averaged, spanwise flow angle distribution; the design intent was 70°. Figure 18(b) shows the vane efficiency as it varies spanwise from 85 to 98 percent.

Figure 19(a) presents the total pressure ratio contours in the stator exit plane. The survey covers approximately 15°, and it captures about 1 1/2 vane pitches. The contours show a low-loss core flow, a clearly defined wake, and a region of considerable total pressure loss near both endwalls. The loss patterns are not symmetric about the midplane. Figure 19(b) shows the efficiency calculated in the stator exit plane. As seen in the previous pressure loss figure, the efficiency is high in the core region whereas losses occur near the endwalls.

Rotor I With Stator II

The mass flow as a function of the inlet-to-exit total pressure ratio for the rotor I-stator II configuration is shown in figure 20. The mass flow at the design speed and pressure ratio is 2.34 lb_m/sec, which is within 1/2 percent of the design value. Data show that the turbine stage chokes at a pressure ratio of 5.0 for most speeds although choking may occur earlier for 90 percent speed. Even with the closed-down stator II, the maximum mass flow is still affected by the rotor speed, indicating a rotor rather than stator choke.
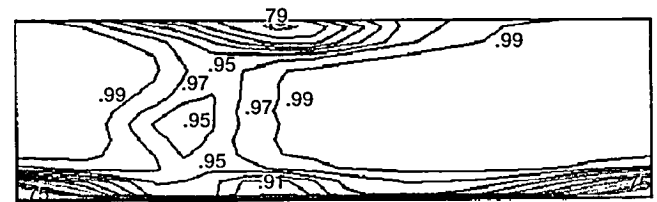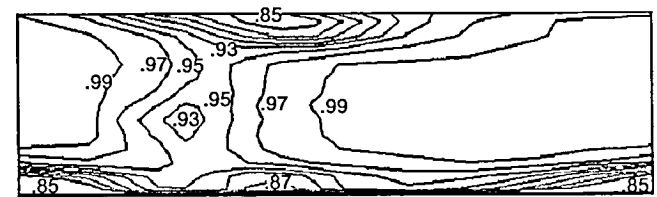
(a)   1 blade passage

(b)   1 blade passage

Figure 19.—Stator exit plane contours for design flow conditions. (a) Total pressure ratio. (b) Efficiency.
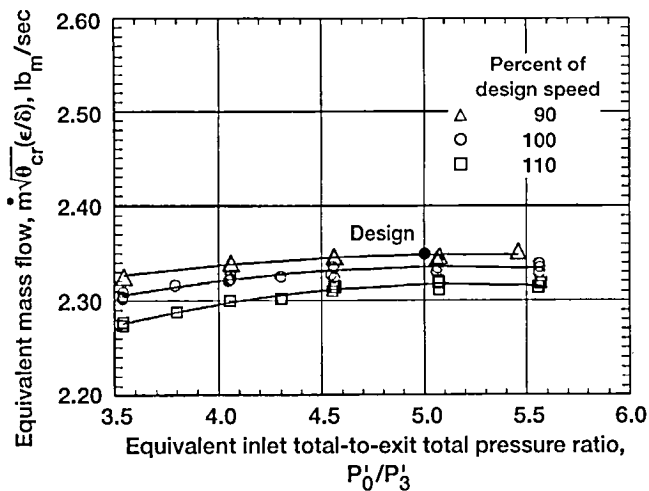
Figure 20.—Variation of mass flow rate with total-to-total pressure ratio for lines of constant speed for rotor I-stator II configuration.
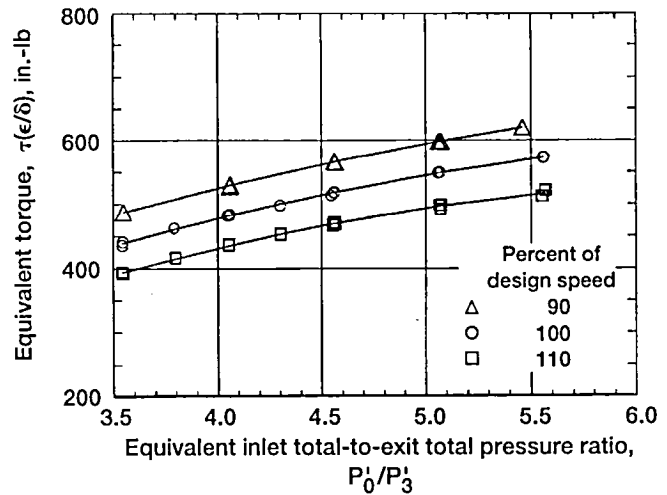
Figure 22.—Variation of turbine torque with total-to-total pressure ratio for lines of constant speed for rotor I-stator II configuration.
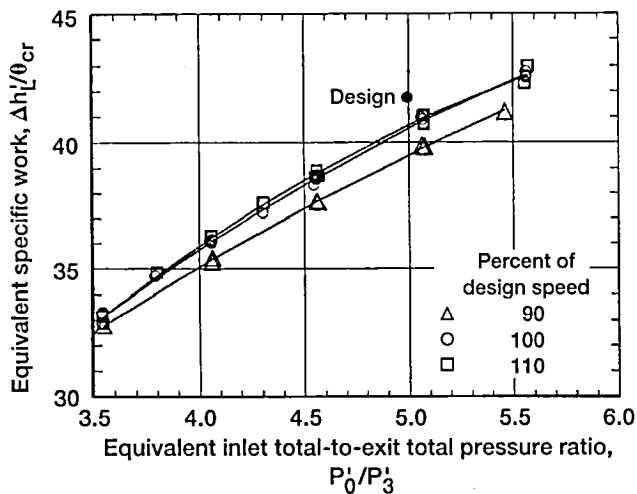
Figure 21.—Variation of specific work with total-to-total pressure ratio for lines of constant speed for rotor I-stator II configuration.

Figure 21 shows the specific work as it varies with the pressure ratio for three speeds. These results are similar to those for the rotor I-stator I test.

Figure 22 presents the corrected torque as a function of the stage pressure ratio for the three speeds. The torque measured at the design pressure ratio and speed was 549 in.-lb, 5 percent less than that for the rotor I-stator I test. As in the previous test, limit loading did not occur for the rotor I-stator II configuration.

In figure 23, the torque measurements were used to show the total efficiency of the rotor. At the design point, the efficiency was 0.885, the same as that for the rotor I-stator I test

and 2.5 points lower than the design value of 91 percent. The trends for the 100- and 110-percent speed lines between the first and second vane angle setting are the same, although the 90-percent speed line shows a lower overall efficiency. The peak efficiency of 0.89 occurred at 110-percent speed and at a pressure ratio of 5.5.

Figure 24 shows the static pressure drop through the stage from stations 0 to 4. A similar pressure drop occurred in the two tests, about 50 percent of the static pressure drop being in the stator and rotor.
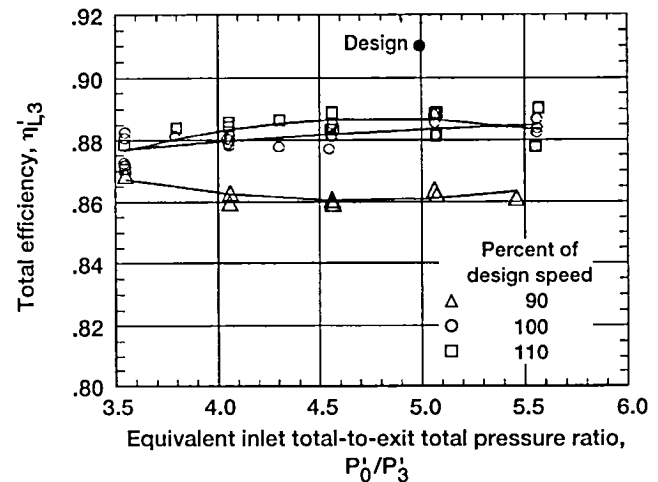
Figure 23.—Variation of total efficiency with total-to-total pressure ratio for lines of constant speed for rotor I-stator II configuration.

13
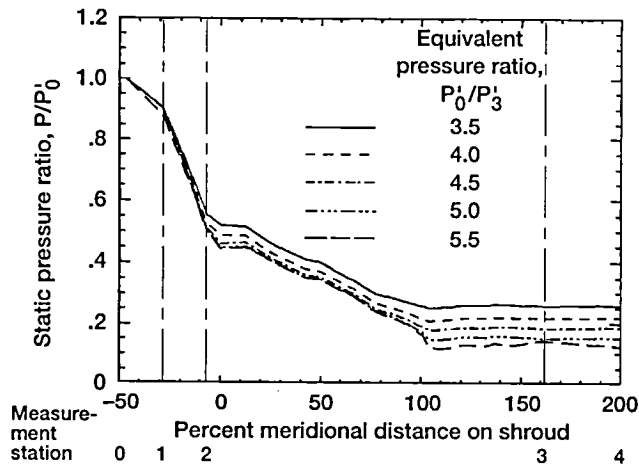
Figure 24.—Shroud static pressures over flow path for rotor I-stator II configuration.

Rotor II With Stator II

Rotor II was tested only with stator II and is slightly shorter axially than rotor I. The overall performance was measured for speeds of 80, 90, 100, 110, and 120 percent of design and at pressure ratios ranging from 3.5 to 5.5.

As shown in figure 25 in the map of the mass flow versus pressure ratio, rotor II exhibited similar behavior to rotor I with the restaggered stator vanes. Speed lines of 80, 90, 100, 110, and 120 percent of design speed are shown. As the pressure ratio is increased, the rotor chokes for each speed at a different mass flow. The design mass flow of 2.36 lb_m/sec was achieved in this configuration.

Figure 26 shows the specific work versus the pressure ratio for various speed lines. For a given pressure ratio, maximum work occurs at speeds of 110 and 120 percent.

Torque is presented in figure 27 as a function of the pressure ratio. The torque measured at the design speed and pressure ratio is approximately 577 in.-lb, slightly higher than that of rotor I. Limit loading did not occur in this range of data.

In figure 28, the stage efficiency for the rotor II-stator II configuration is shown as it varies with the pressure ratio for various speed lines. At the design pressure ratio and speed, the total efficiency was 0.88, which was a half point lower than that of the rotor I-stator I configuration.

Rotor exit surveys were obtained for rotor II. Compared with rotor I, rotor II had a slight difference in spanwise flow. Figure 29 shows the spanwise variation of the flow angle at the rotor exit.

Figure 30 shows the temperature variation from hub to tip for rotor II. The temperature variation shows a slightly different trend than that of rotor I.

Figure 31 presents the spanwise distribution of the inlet-to-exit total pressure ratio at the rotor exit. These data show

slightly less pressure drop than that observed in the rotor I configurations.

Figure 32 shows the efficiency calculated by using the temperature drop from inlet-to-the-exit survey rake position as it traversed from hub to tip. As noted for the previous configurations, the efficiency is highest towards the hub and lowest at the tip region.
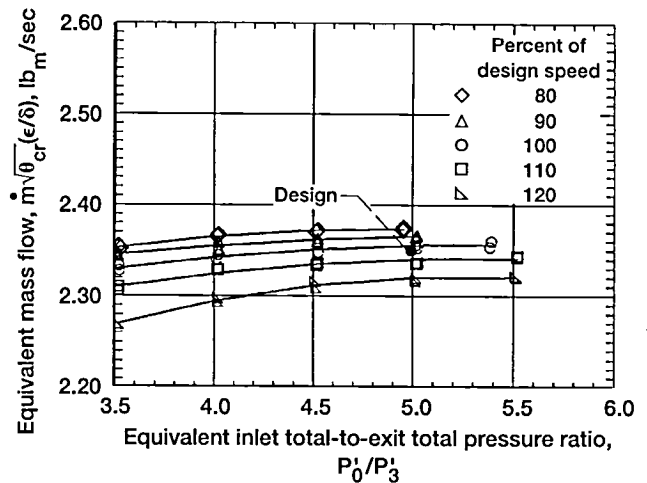
Figure 25.—Variation of mass flow rate with total-to-total pressure ratio for lines of constant speed for rotor I-stator II configuration.
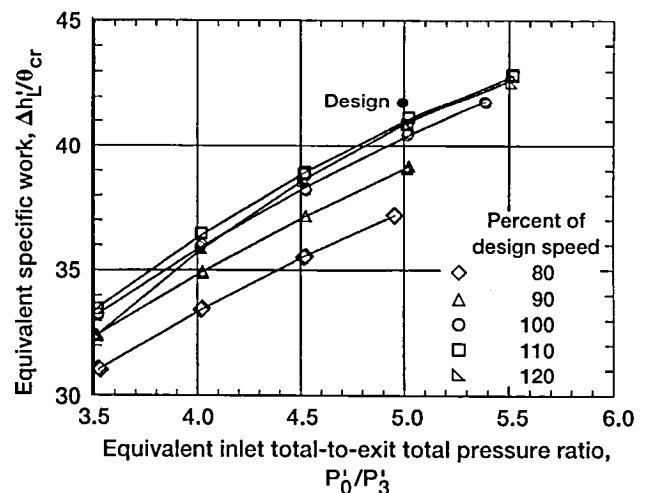
Figure 26.—Variation of specific work with total-to-total pressure ratio for lines of constant speed for rotor II-stator II configuration.

The static-to-total inlet pressure ratio is shown in figure 33 as it varies through the rotor II-stator II configuration at the design speed. This configuration has a slightly higher pressure drop in the stator than in the rotor (i.e., a lower rotor reaction).
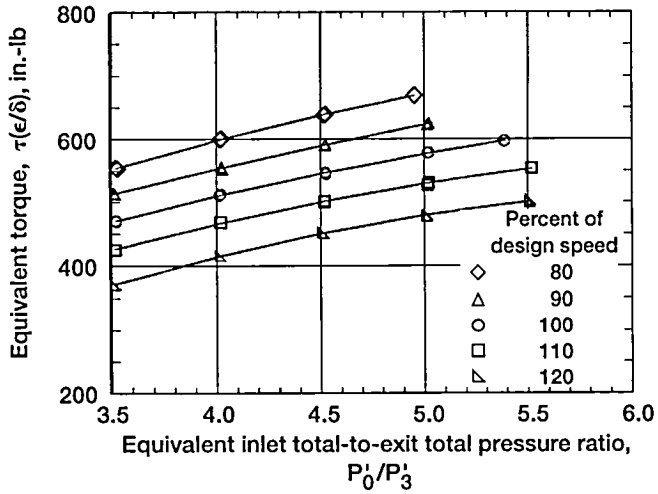
Figure 27.—Variation of turbine torque with total-to-total pressure ratio for lines of constant speed for rotor II-stator II configuration.
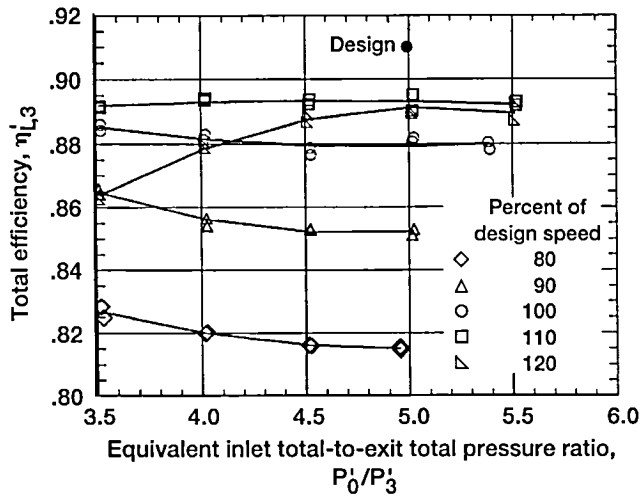
Figure 28.—Variation of total efficiency with total-to-total pressure ratio for lines of constant speed for rotor II-stator II configuration.
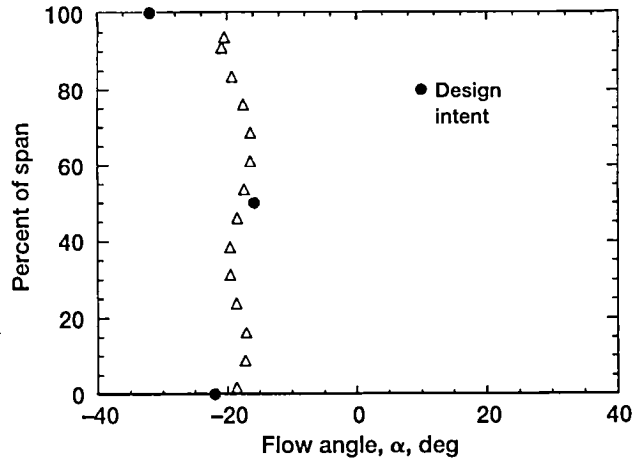
Figure 29.—Radial variation of exit flow angle at design operating condition for rotor II-stator II configuration.
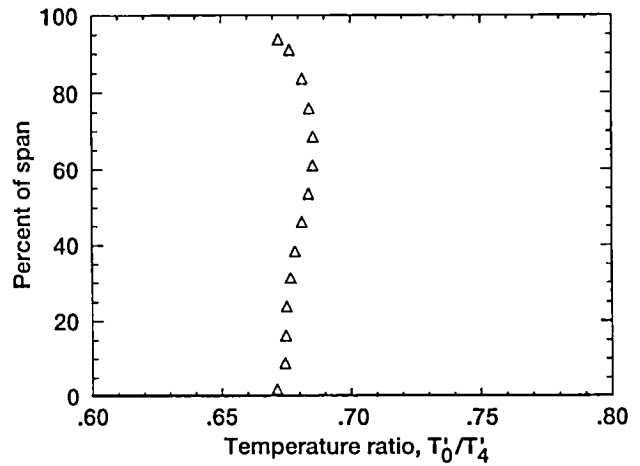
Figure 30.—Radial variation of exit-to-inlet total temperature ratio at design operating condition for rotor II-stator II configuration.

15
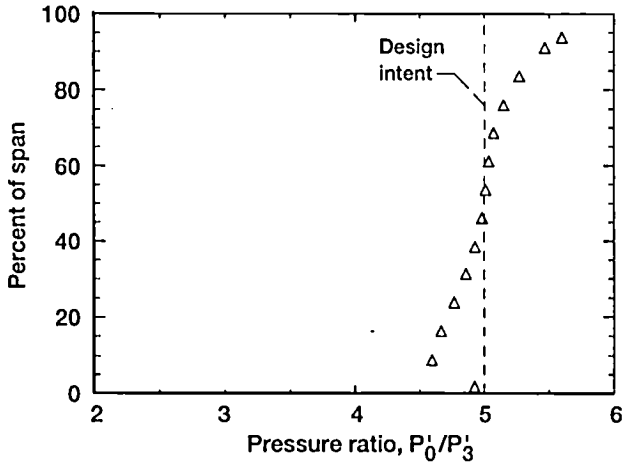
Figure 31.—Radial variation of exit-to-inlet total pressure ratio at design operating condition for rotor II-stator II configuration.
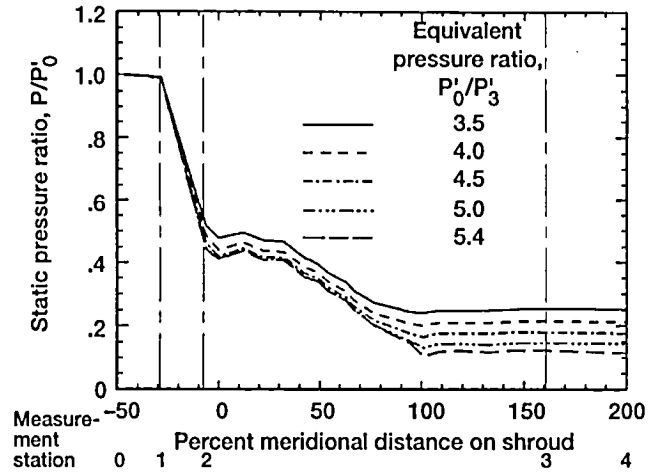
Figure 33.—Shroud static pressures over flow path for rotor II-stator II configuration.
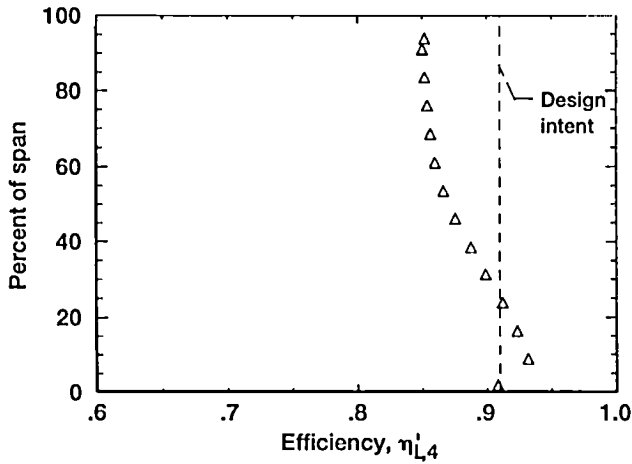
Figure 32.—Radial variation of total efficiency measured at rotor exit at design operating condition for rotor II-stator II configuration.
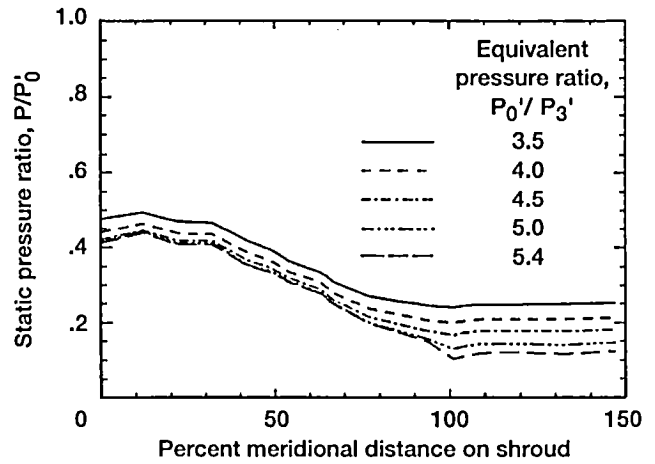
Figure 34.—Shroud static pressures over rotor II for various pressure ratios at design rotor speed.

16

The wall static pressure changes are shown from the rotor inlet to exit in figure 34 for the design speed line and at various pressure ratios. Compared with rotor I, rotor II had less of a static pressure drop as the flow went from the inducer to the exducer; there was less acceleration occurring in the flow for the shorter rotor II.

Discussion

The efficiencies measured in this investigation were 2 to 3 percent below the design intent. To address this discrepancy, analytical studies were conducted by using the compact turbine experiment to predict the losses; the results are presented in references 2 and 3. The analytical study shows that the major losses are caused by incidence and clearance. Further studies are needed to determine how to avoid some losses due to the clearance between the blades and the backface where the turbine is scalloped. Another area to study is the incidence loss due to the leading edge geometry.

When the compact turbine designs are compared with state-of-the-art turbines described in the literature, the compact turbines met and, in most cases, exceeded the efficiencies measured thus far for conventional turbines. For example, figure 35 shows state-of-the-art radial turbine data (refs. 7 to 13), which were in the 3119-hp range.

pressure ratio, specific work, efficiency, work factor, and torque. The results of the stator and rotor exit surveys were presented along with the rotor exit rake data. The results obtained from the three configurations were nearly identical. The efficiencies measured for these designs were approximately 2 to 3 points lower than the design intent. However, when the compact turbine designs were compared with the state-of-the-art turbines reported in the literature, the compact turbines met and, in most cases, exceeded the efficiencies demonstrated to date.

This investigation showed that a relatively shorter high-work radial inflow turbine rotor can achieve the high efficiencies relative to high-work baseline design turbines. A size reduction of up to 52 percent in axial length, 4 percent in radial width, and 40 percent in weight can be achieved without a major efficiency penalty.

Lewis Research Center
National Aeronautics and Space Administration
Cleveland, Ohio, January 11, 1995
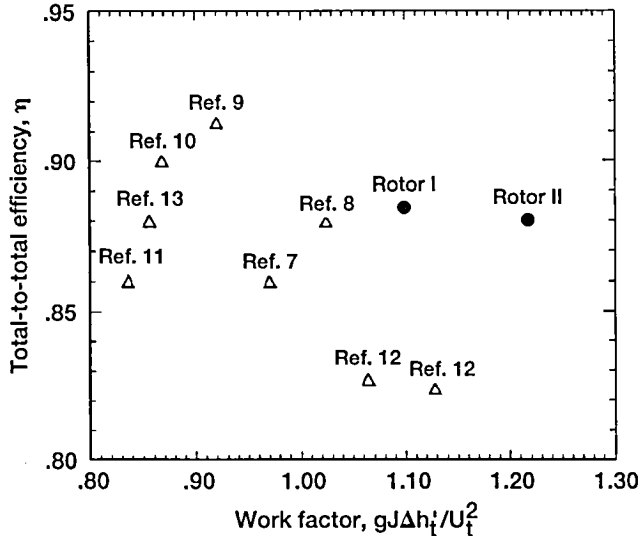
Figure 35.—Comparison of compact turbines to state-of-the-art turbines described in literature.

Summary of Results

An experimental performance evaluation of three compact radial inflow turbine stage configurations was conducted. The overall performance was presented in terms of mass flow,

Appendix A

Geometry

Side view

Stator

X1 — X2

Leading edge
(R = 7.23 in.)

Shroud

Hub

Rotor

Trailing
edge

C_L

X

Forward looking aft

36 Vanes

θ_s

θ_s

θ_p

14 Blades

θ

Aft looking forward

Rotation

R

Rθ
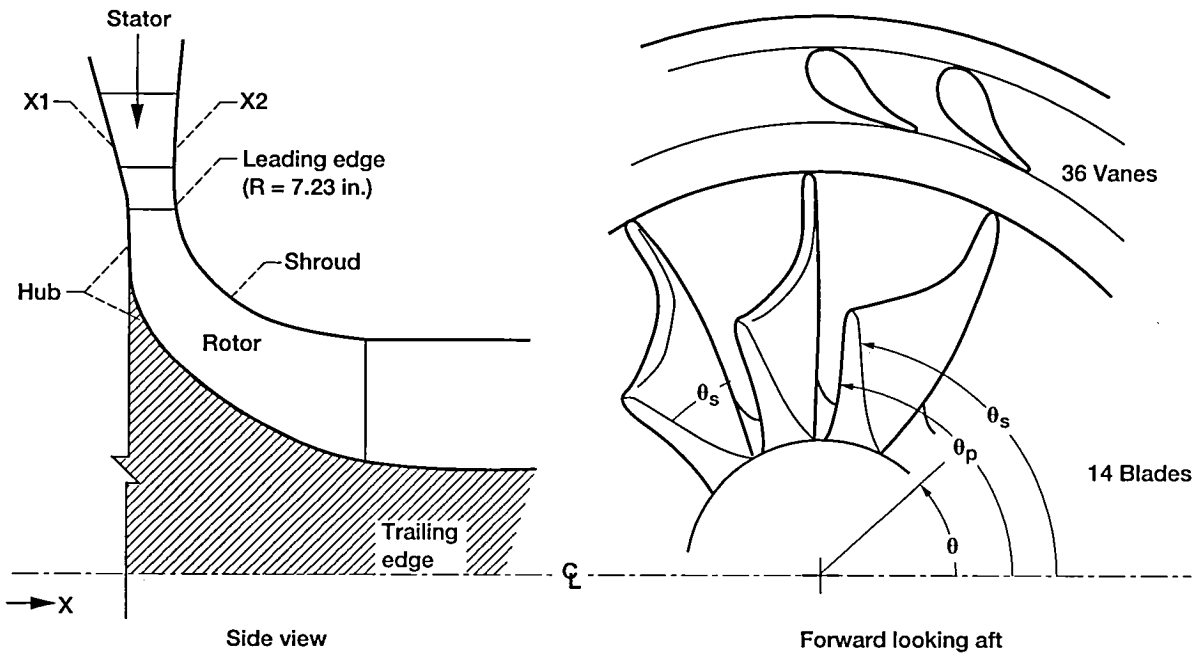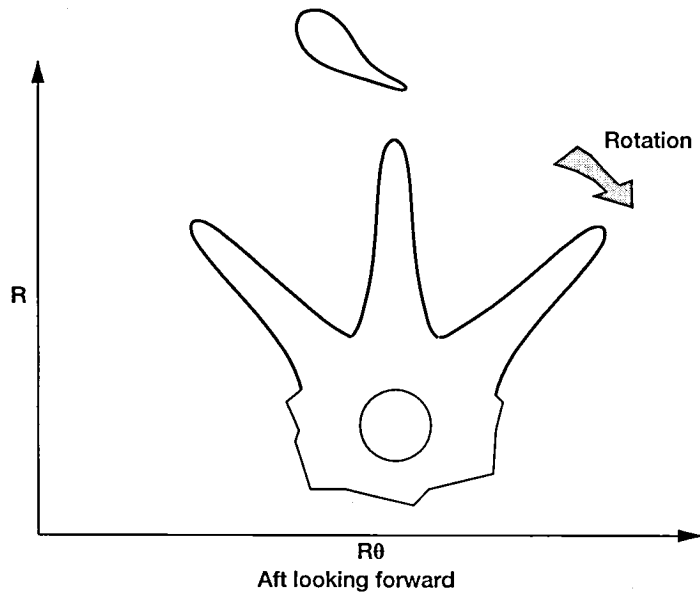
Defining coordinates

TABLE II.—INLET GUIDE VANE ENDWALL
COORDINATES

R, in.	$X1$,[a] in.	$X2$,[a] in.
10.52110	-0.39152	0.91757
9.01806	-0.17754	0.70359
8.83000	-0.15077	0.67682
8.59850	-0.11781	0.64386
8.36701	-0.08485	0.61090
8.13551	-0.05189	0.57794
7.90402	-0.01893	0.54498
7.78827	-0.00245	0.52850
7.73040	0.00579	0.52027
7.67252	0.01402	0.51203
7.66509	0.01503	0.51102
7.65666	0.01602	0.51003
7.64665	0.01703	0.50902
7.63359	0.01802	0.50803
7.60200	0.01903	0.50700

[a]X-offset = -0.28206 in.

TABLE III.—INLET GUIDE VANE GEOMETRY:
STATOR I CONFIGURATION

R, in.	Θ_p, rad	Θ_s, rad
8.83000	-0.16035	-0.16035
8.82735	-0.15777	-0.16296
8.82471	-0.15672	-0.16405
8.82207	-0.15593	-0.16489
8.81943	-0.15526	-0.16559
8.81679	-0.15468	-0.16621
8.80359	-0.15246	-0.16862
8.79042	-0.15083	-0.17045
8.77726	-0.14951	-0.17198
8.76413	-0.14840	-0.17344

TABLE III.—Continued.

R, in.	Θ_p, rad	Θ_s, rad
8.75102	-0.14735	-0.17485
8.73793	-0.14629	-0.17621
8.72485	-0.14523	-0.17753
8.71180	-0.14416	-0.17880
8.69876	-0.14309	-0.18003
8.66625	-0.14038	-0.18291
8.63388	-0.13764	-0.18549
8.60161	-0.13486	-0.18779
8.56947	-0.13204	-0.18980
8.53745	-0.12919	-0.19152
8.50555	-0.12629	-0.19294
8.47377	-0.12334	-0.19404
8.44210	-0.12035	-0.19484
8.41056	-0.11732	-0.19531
8.37913	-0.11423	-0.19545
8.34783	-0.11108	-0.19524
8.31663	-0.10789	-0.19467
8.28556	-0.10463	-0.19372
8.25459	-0.10131	-0.19237
8.22375	-0.09792	-0.19060
8.19302	-0.09446	-0.18839
8.16241	-0.09093	-0.18569
8.13191	-0.08732	-0.18247
8.10153	-0.08362	-0.17869
8.07125	-0.07983	-0.17428
8.04109	-0.07593	-0.16916
8.01105	-0.07193	-0.16326
7.98112	-0.06782	-0.15644
7.95129	-0.06357	-0.14855
7.92158	-0.05918	-0.13941

20

TABLE III.—Concluded.

R, in.	Θ_p, rad	Θ_s, rad
7.89198	-0.05463	-0.12906
7.86249	-0.04991	-0.11771
7.83311	-0.04500	-0.10566
7.80384	-0.03985	-0.09312
7.77468	-0.03445	-0.08027
7.74563	-0.02875	-0.06719
7.71669	-0.02269	-0.05369
7.69362	-0.01754	-0.04330
7.67061	-0.01205	-0.03258
7.64767	-0.00615	-0.02182
7.62480	0.00025	-0.01102
7.61339	0.00148	-0.00562
7.60200	0.00000	0.00000

TABLE IV.—INLET GUIDE VANE GEOMETRY: STATOR II CONFIGURATION

R_p, in.	Θ_p, rad	R_s, in.	Θ_s, rad
8.82652	-0.16183	8.82652	-0.16183
8.82429	-0.15925	8.82345	-0.16444
8.82182	-0.15820	8.82064	-0.16553
8.81930	-0.15740	8.81786	-0.16636
8.81676	-0.15673	8.81511	-0.16705
8.81422	-0.15614	8.81237	-0.16767
8.80138	-0.15389	8.79879	-0.17006
8.78847	-0.15224	8.78533	-0.17186
8.77553	-0.15089	8.77193	-0.17336
8.76258	-0.14975	8.75857	-0.17479
8.74964	-0.14867	8.74523	-0.17618
8.73672	-0.14758	8.73192	-0.17751
8.72381	-0.14649	8.71863	-0.17880

TABLE IV.—Continued.

R_p, in.	Θ_p, rad	R_s, in.	Θ_s, rad
8.71093	-0.14540	8.70538	-0.18005
8.69807	-0.14430	8.69215	-0.18125
8.66600	-0.14152	8.65919	-0.18406
8.63407	-0.13871	8.62640	-0.18658
8.60226	-0.13587	8.59378	-0.18881
8.57057	-0.13298	8.56131	-0.19075
8.53902	-0.13005	8.52903	-0.19240
8.50759	-0.12708	8.49691	-0.19375
8.47628	-0.12407	8.46496	-0.19478
8.44510	-0.12101	8.43317	-0.19551
8.41405	-0.11790	8.40155	-0.19591
8.38312	-0.11475	8.37011	-0.19597
8.35233	-0.11153	8.33884	-0.19569
8.32165	-0.10827	8.30774	-0.19505
8.29110	-0.10494	8.27683	-0.19403
8.26068	-0.10155	8.24609	-0.19261
8.23038	-0.09809	8.21554	-0.19077
8.20021	-0.09457	8.18516	-0.18848
8.17017	-0.09096	8.15499	-0.18570
8.14026	-0.08728	8.12501	-0.18241
8.11047	-0.08351	8.09524	-0.17855
8.08081	-0.07965	8.06568	-0.17406
8.05128	-0.07569	8.03634	-0.16887
8.02188	-0.07162	8.00725	-0.16289
7.99261	-0.06744	7.97842	-0.15600
7.96346	-0.06312	7.94986	-0.14803
7.93446	-0.05867	7.92162	-0.13881
7.90559	-0.05405	7.89369	-0.12839
7.87687	-0.04927	7.86603	-0.11697
7.84827	-0.04428	7.83858	-0.10485

TABLE IV.—Concluded.

R_p, in.	Θ_p, rad	R_s, in	Θ_s, rad
7.81983	-0.03907	7.81133	-0.09225
7.79154	-0.03361	7.78423	-0.07934
7.76340	-0.02785	7.75727	-0.06620
7.73543	-0.02173	7.73045	-0.05292
7.71318-	0.01652	7.70908	-0.04222
7.69105	-0.01099	7.68779	-0.03146
7.66905-	0.00505	7.66656	-0.02067
7.64720	0.00140	7.64541	-0.00984
7.63598	0.00266	7.63486	-0.00442
7.62436	0.00121	7.62436	0.00121

TABLE V.—COMPACT ROTOR I BLADE COORDINATES AT SHROUDS

X, in.	R, in.	Θ_s, rad	Θ_p, rad
0.26303	7.22948	0.00000	0.00000
0.26303	7.22197	0.00351	-0.00351
0.26303	7.21446	0.00493	-0.00493
0.26303	7.19943	0.00689	-0.00689
0.26303	7.16937	0.00949	-0.00949
0.26303	7.13930	0.01130	-0.01130
0.26303	7.10923	0.01266	-0.01266
0.26303	7.07918	0.01369	-0.01369
0.26303	7.04912	0.01447	-0.01447
0.26303	7.01906	0.01503	-0.01503
0.26303	6.98899	0.01539	-0.01539
0.26303	6.95893	0.01555	-0.01555
0.26303	6.92887	0.01562	-0.01562
0.26378	6.89751	0.01569	-0.01569
0.26453	6.84072	0.01581	-0.01582
0.26603	6.80471	0.01589	-0.01590

TABLE V.—Continued.

X, in.	R, in.	Θ_s, rad	Θ_p, rad
0.26754	6.77709	0.01595	-0.01596
0.26904	6.75384	0.01599	-0.01601
0.27054	6.73302	0.01604	-0.01606
0.27806	6.65319	0.01618	-0.01626
0.28557	6.59231	0.01628	-0.01644
0.29309	6.54125	0.01634	-0.01663
0.30060	6.49640	0.01639	-0.01683
0.30812	6.45610	0.01641	-0.01705
0.31563	6.41921	0.01641	-0.01728
0.32315	6.38504	0.01639	-0.01752
0.33066	6.35303	0.01635	-0.01778
0.33818	6.32289	0.01630	-0.01805
0.37575	6.19249	0.01567	-0.01957
0.41333	6.08456	0.01446	-0.02128
0.45090	5.99121	0.01275	-0.02329
0.48848	5.90824	0.01066	-0.02564
0.52605	5.83330	0.00823	-0.02840
0.56363	5.74469	0.00550	-0.03157
0.60120	5.70137	0.00250	-0.03516
0.63878	5.64249	-0.00077	-0.03917
0.67635	5.58745	-0.00430	-0.04361
0.71393	5.53576	-0.00810	-0.04846
0.75150	5.48702	-0.01215	-0.05371
0.78908	5.44096	-0.01647	-0.05937
0.82666	5.39728	-0.02107	-0.06541
0.86423	5.35582	-0.02596	-0.07183
0.90181	5.31636	-0.03116	-0.07861
0.93938	5.27875	-0.03668	-0.08575
0.97231	5.24725	-0.04183	-0.09224
1.00602	5.21612	-0.04737	-0.09920

TABLE V.—Concluded.

X, in.	R, in.	Θ_s, rad	Θ_p, rad
1.04034	5.18559	-0.05330	-0.10650
1.07518	5.15562	-0.05978	-0.11421
1.11054	5.12619	-0.06668	-0.12216
1.14643	5.09728	-0.07418	-013061
1.18282	5.06888	-0.08222	-0.13929
1.21969	5.04100	-0.09088	-0.14848
1.25704	5.01357	-0.10008	-0.15802
1.29487	4.98668	~0.11003	-0.16800
1.33318	4.96033	-0.12064	-0.17846
1.37196	4.93445	-0.13202	-0.18939
1.41122	4.90917	-0.14419	-0.20094
1.45094	4.88442	-0.15703	-0.21320
1.49115	4.86029	-0.17071	-0.22582
1.53182	4.83679	-0.18516	-0.23907
1.57297	4.81399	-0.20045	-0.25289
1.61459	4.79193	-0.21643	-0.26705
1.65666	4.77070	-0.23321	-0.28189
1.69920	4.75038	-0.25061	-0.29684
1.74218	4.73110	-0.26873	-0.31219
1.78559	4.71297	-0.28758	-0.32779
1.82937	4.69623	-0.30699	-0.34357
1.84291	4.69136	-0.31303	-0.34853
1.89397	4.67447	-0.33631	-0.36704
1.94538	4.65907	-0.35999	-0.38568
1.99705	4.64507	-0.38417	-0.40433
2.04898	4.63198	-0.40897	-0.42320
2.06664	4.62775	-0.41742	-0.42962
2.07000	4.64200	-0.41742	-0.42962

TABLE VI.—COMPACT ROTOR I: HOT SECTION II

X, in.	R, in.	Θ_s, rad	Θ_p, rad
0.13151	7.22948	0.00000	0.00000
0.13151	7.22197	0.00351	-0.00351
0.13151	7.21446	0.00493	-0.00493
0.13151	7.19943	0.00689	-0.00689
0.13151	7.16937	0.00949	-0.00949
0.13151	7.13930	0.01130	-0.01130
0.13151	7.10923	0.01266	-0.01266
0.13151	7.07918	0.01369	-0.01369
0.13151	7.04912	0.01447	-0.01447
0.13151	7.01906	0.01503	-0.01503
0.13151	6.98899	0.01539	-0.01539
0.13151	6.95893	0.01555	-0.01555
0.13151	6.92887	0.01573	-0.01573
0.13226	6.87527	0.01613	-0.01613
0.13377	6.76804	0.01718	-0.01718
0.13542	6.71633	0.01769	-0.01769
0.14294	6.56288	0.01928	-0.01928
0.15045	6.46045	0.02051	-0.02051
0.15797	6.37927	0.02162	-0.02162
0.16548	6.31057	0.02254	-0.02254
0.17300	6.25033	0.02346	-0.02346
0.18051	6.19635	0.02432	-0.02432
0.23297	5.91534	0.02945	-0.02945
0.26303	5.79693	0.03210	-0.03210
0.27054	5.77028	0.03271	-0.03273
0.27806	5.74461	0.03324	-0.03332
0.28557	5.71985	0.03370	-0.03387
0.33818	5.56713	0.03543	-0.03719
0.39078	5.44115	0.03524	-0.04021
0.44339	5.33387	0.03377	-0.04350
0.49599	5.24051	0.03135	-0.04731
0.54860	5.15806	0.02821	-0.05183
0.60120	5.08440	0.02447	-0.05713
0.65381	5.01799	0.02021	-0.06326
0.70641	4.95772	0.01519	-0.06995
0.75902	4.90271	0.00934	-0.07713
0.81163	4.85223	0.00270	-0.08484
0.86423	4.80575	-0.00471	-0.09307

TABLE VI.—Concluded.

X, in.	R, in.	Θ_s, rad	Θ_p, rad
0.91684	4.76280	-0.01289	-0.10186
0.96944	4.72300	-0.02184	-0.11120
1.02205	4.68602	-0.03159	-0.12110
1.07465	4.65160	-0.04217	-0.13157
1.12726	4.61952	-0.05361	-0.14259
1.17986	4.58954	-0.06597	-0.15419
1.23247	4.56150	-0.07931	-0.16636
1.28507	4.53527	-0.09372	-0.17910
1.33768	4.51065	-0.10927	-0.19249
1.39028	4.48758	-0.12600	-0.20649
1.44289	4.46592	-0.14391	-0.22121
1.49549	4.44557	-0.16295	-0.23666
1.54810	4.42648	-0.18302	-0.25279
1.60070	4.40852	-0.20402	-0.26952
1.65331	4.39166	-0.22585	-0.28678
1.70592	4.37582	-0.24837	-0.30446
1.75852	4.36092	-0.27150	-0.32250
1.81113	4.34692	-0.29514	-0.34080
1.86373	4.33380	-0.31921	-0.35932
1.91634	4.32147	-0.34364	-0.37802
1.96894	4.30989	-0.36838	-0.39685
2.02155	4.29906	-0.39338	-0.41578
2.07415	4.28890	-0.41860	-0.43481
2.08377	4.28712	-0.42323	-0.43830

TABLE VII.—COMPACT ROTOR I: HOT SECTION III

X, in.	R, in.	Θ_s, rad	Θ_s, rad
0.0	7.33948	0.00	0.00
0.0	7.22197	0.00351	-0.00351
0.0	7.21446	0.00493	-0.00493
0.0	7.19943	0.00689	-0.00689
0.0	7.16937	0.00949	-0.00949
0.0	7.13930	0.01130	-0.01130
0.0	7.10923	0.01266	-0.01266
0.0	7.07918	0.01369	-0.01369
0.0	7.04912	0.01447	-0.01447
0.0	7.01906	0.01503	-0.01503

TABLE VII.—Continued.

X, in.	R, in.	Θ_s, rad	Θ_s, rad
0.0	6.98899	0.01539	-0.01539
0.0	6.95893	0.01555	-0.01555
0.0	6.92887	0.01573	-0.01573
0.00075	6.85058	0.01637	-0.01637
0.00150	6.77232	0.01713	-0.01713
0.00301	6.70272	0.01783	-0.01783
0.00451	6.64999	0.01836	-0.01836
0.00601	6.60606	0.01882	-0.01882
0.00767	6.56530	0.01925	-0.01925
0.01518	6.41918	0.02106	-0.02106
0.02270	6.31054	0.02254	-0.02254
0.03021	6.22141	0.02392	-0.02392
0.03773	6.14463	0.02512	-0.02512
0.04524	6.07676	0.02639	-0.02639
0.05276	6.01553	0.02745	-0.02745
0.10536	5.69448	0.03463	-0.03463
0.15797	5.47124	0.04120	-0.04120
0.21042	5.29776	0.04725	-0.04725
0.26303	5.15561	0.05305	-0.05305
0.31563	5.03535	0.05769	-0.05856
0.36824	4.93142	0.06058	-0.06398
0.42084	4.84023	0.06189	-0.06940
0.47345	4.75928	0.06175	-0.07486
0.52605	4.68678	0.06025	-0.08041
0.57866	4.62138	0.05747	-0.08609
0.63126	4.56204	0.05347	-0.09191
0.68387	4.50793	0.04831	-0.09790
0.73647	4.45839	0.04207	-0.10412
0.78908	4.41291	0.03481	-0.11065
0.84169	4.37099	0.02659	-0.11751
0.89429	4.33230	0.01742	-0.12474
0.94690	4.29649	0.00734	-0.13238
0.99950	4.26332	-0.00365	-0.14045
1.05211	4.23250	-0.01555	-0.14899
1.10471	4.20386	-0.02836	-0.15803
1.15732	4.17721	-0.04209	-0.16762
1.20992	4.15240	-0.05675	-0.17779
1.26253	4.12928	-0.07236	-0.18861

TABLE VII.—Concluded.

X, in.	R, in.	Θ_s, rad	Θ_s, rad
1.31513	4.10773	-0.08895	-0.20021
1.36774	4.08762	-0.10653	-0.21255
1.42034	4.06886	-0.12514	-0.22577
1.47295	4.05138	-0.14480	-0.23980
1.52555	4.03507	-0.16548	-0.25461
1.57816	4.01987	-0.18707	-0.27013
1.63076	4.00570	-0.20946	-0.28626
1.68337	3.99252	-0.23252	-0.30295
1.73598	3.98024	-0.25614	-0.32012
1.78858	3.96885	-0.28019	-0.33769
1.84119	3.95825	-0.30461	-0.35560
1.89379	3.94845	-0.32931	-0.37381
1.94640	3.93937	-0.35424	-0.39227
1.99900	3.93099	-0.37935	-0.41094
2.05161	3.92328	-0.40461	-0.42980
2.06664	3.92119	-0.41185	-0.43521
2.10046	3.91666	-0.42818	-0.44746

TABLE VIII.—COMPACT ROTOR I: HOT SECTION IV

X, in.	R, in.	Θ_s, rad	Θ_p, rad
-0.13151	7.22948	0.0	0.0
-0.13151	7.22197	0.00351	-0.00351
-0.13151	7.21446	0.00493	-0.00493
-0.13151	7.19943	0.00689	-0.00689
-0.13151	7.16937	0.00949	-0.00949
-0.13151	7.13930	0.01130	-0.01130
-0.13151	7.10923	0.01266	-0.01266
-0.13151	7.07918	0.01369	-0.01369
-0.13151	7.04912	0.01447	-0.01447
-0.13151	7.01906	0.01503	-0.01503
-0.13151	6.98899	0.01539	-0.01539
-0.13151	6.95893	0.01555	-0.01555
-0.13151	6.92887	0.01573	-0.01573
-0.13076	6.81072	0.01676	-0.01676
-0.12926	6.71139	0.01774	-0.01774
-0.12761	6.63863	0.01849	-0.01849
-0.12009	6.42752	0.02097	-0.02097

TABLE VIII.—Continued.

X, in.	R, in.	Θ_s, rad	Θ_p, rad
-0.11258	6.28653	0.02292	-0.02292
-0.10506	6.17494	0.02462	-0.02462
-0.09755	6.08063	0.02631	-0.02631
-0.09003	5.99805	0.02780	-0.02780
-0.08252	5.92413	0.02927	-0.02927
-0.02991	5.54092	0.03893	-0.03893
0.02270	5.27627	0.04812	-0.04812
0.07530	5.07087	0.05697	-0.05697
0.12791	4.90254	0.06564	-0.06564
0.18051	4.76005	0.07513	-0.07513
0.23297	4.63689	0.08388	-0.08388
0.26303	4.57347	0.08866	-0.08866
0.27054	4.55830	0.08982	-0.08984
0.27806	4.54341	0.09093	-0.09101
0.28557	4.52876	0.09199	-0.09216
0.33818	4.43282	0.09800	-0.09976
0.39078	4.34690	0.10179	-0.10676
0.44339	4.26946	0.10356	-0.11329
0.49599	4.19925	0.10350	-0.11946
0.54860	4.13534	0.10175	-0.12537
0.60120	4.07693	0.09842	-0.13108
0.65381	4.02339	0.09360	-0.13665
0.70641	3.97417	0.08737	-0.14215
0.75902	3.92885	0.07985	-0.14765
0.81163	3.88705	0.07109	-0.15323
0.86423	3.84847	0.06116	-0.15894
0.91684	3.81278	0.05009	-0.16484
0.96944	3.77975	0.03792	-0.17097
1.02205	3.74918	0.02468	-0.17738
1.07465	3.72090	0.01039	-0.18412
1.12726	3.69468	-0.00494	-0.19126
1.17986	3.67044	-0.02130	-0.19885
1.23247	3.64798	-0.03869	-0.20698
1.28507	3.62724	-0.05709	-0.21572
1.33768	3.60808	-0.07649	-0.22526
1.39028	3.59040	-0.09685	-0.23564
1.44289	3.57411	-0.11807	-0.24705
1.49549	3.55911	-0.14007	-0.25953

TABLE VIII.—Concluded.

X, in.	R, in.	Θ_s, rad	Θ_p, rad
1.54810	3.54537	-0.16276	-0.27304
1.60070	3.53279	-0.18604	-0.28751
1.65331	3.52133	-0.20982	-0.30281
1.70592	3.51089	-0.23403	-0.31881
1.75852	3.50146	-0.25858	-0.33542
1.81113	3.49296	-0.28344	-0.35251
1.86373	3.48537	-0.30853	-0.37000
1.91634	3.47863	-0.33382	-0.38784
1.96894	3.47270	-0.35927	-0.40596
2.02155	3.46755	-0.38485	-0.42431
2.07415	3.46311	-0.41054	-0.44288
2.08167	3.46256	-0.41420	-0.44555
2.08918	3.46200	-0.41788	-0.44822
2.09670	3.46145	-0.42156	-0.45090
2.10421	3.46092	-0.42524	-0.45357
2.11173	3.46041	-0.42891	-0.45626
2.11924	3.45990	-0.43260	-0.45894
2.12120	3.45976	-0.43356	-0.45964

TABLE IX.—ROTOR I BLADE COORDINATES AT HUB

X, in.	R, in.	Θ_s, rad	Θ_p, rad
-0.26303	7.22948	0.00000	0.00000
-0.26303	7.22197	0.00351	-0.00351
-0.26303	7.21446	0.00493	-0.00493
-0.26303	7.19943	0.00689	-0.00689
-0.26303	7.16937	0.00949	-0.00949
-0.26303	7.13930	0.01130	-0.01130
-0.26303	7.10923	0.01266	-0.01266
-0.26303	7.07918	0.01369	-0.01369
-0.26303	7.04912	0.01447	-0.01447
-0.26303	7.01906	0.01503	-0.01503
-0.26303	6.98899	0.01539	-0.01539
-0.26303	6.95893	0.01555	-0.01555

TABLE IX.—Continued.

X, in.	R, in.	Θ_s, rad	Θ_p, rad
-0.26303	6.92887	0.01573	-0.01573
-0.26303	6.83869	0.01648	-0.01648
-0.26303	6.76354	0.01722	-0.01722
-0.26303	6.68839	0.01798	-0.01798
-0.26303	6.61324	0.01875	-0.01875
-0.26303	6.46294	0.02046	-0.02046
-0.26303	6.31264	0.02250	-0.02250
-0.26303	6.16234	0.02488	-0.02448
-0.26303	6.01204	0.02750	-0.02750
-0.26303	5.86174	0.03064	-0.03064
-0.26303	5.71144	0.03421	-0.03421
-0.26303	5.56114	0.03838	-0.03838
-0.26303	5.41084	0.04320	-0.04320
-0.26303	5.26053	0.04871	-0.04871
-0.26303	5.18538	0.05174	-0.05174
-0.26303	5.11023	0.05515	-0.05515
-0.26303	5.03508	0.05866	-0.05866
-0.26303	4.95994	0.06258	-0.06258
-0.26303	4.88987	0.06650	-0.06650
-0.25927	4.87595	0.06737	-0.06737
-0.25536	4.86198	0.06829	-0.06829
-0.24785	4.83592	0.07000	-0.07000
-0.24033	4.81101	0.07167	-0.07167
-0.23282	4.78704	0.07328	-0.07328
-0.22530	4.76397	0.07486	-0.07486
-0.21779	4.74170	0.07639	-0.07639
-0.21027	4.72014	0.07790	-0.07790
-0.15767	4.58501	0.08777	-0.08777
-0.10506	4.46973	0.09690	-0.09690
-0.05246	4.36800	0.10564	-0.10564

TABLE IX.—Continued.

X, in.	R, in.	Θ_s, rad	Θ_p, rad
0.00015	4.27636	0.11418	-0.11418
0.05276	4.19266	0.12264	-0.12264
0.10536	4.11549	0.13109	-0.13110
0.15797	4.04377	0.13961	-0.13961
0.21042	3.97678	0.14764	-0.14764
0.26303	3.91396	0.15370	-0.15370
0.31563	3.85480	0.15782	-0.15869
0.36824	3.79898	0.16009	-0.16349
0.42084	3.74618	0.16060	-0.16811
0.47345	3.69616	0.15941	-0.17253
0.52605	3.64872	0.15661	-0.17678
0.57866	3.60363	0.15225	-0.18087
0.63126	3.56083	0.14640	-0.18483
0.68387	3.52011	0.13909	-0.18867
0.73647	3.48141	0.13038	-0.19244
0.78908	3.44461	0.12034	-0.19618
0.84169	3.40961	0.10900	-0.19992
0.89429	3.37636	0.09641	-0.20373
0.94690	3.34481	0.08262	-0.20766
0.99950	3.31484	0.06767	-0.21177
1.05211	3.28647	0.05160	-0.21615
1.10571	3.25959	0.03448	-0.22087
1.15732	3.23421	0.01633	-0.22603
1.20992	3.21026	-0.00281	-0.23173
1.26253	3.18773	-0.02289	-0.23809
1.31513	3.16658	-0.04385	-0.24529
1.36774	3.14682	-0.06567	-0.25341
1.42034	3.12836	-0.08830	-0.26261
1.47295	3.11125	-0.11170	-0.27291
1.52555	3.09542	-0.13577	-0.28432

33

TABLE IX.—Concluded.

X, in.	R, in.	Θ_s, rad	Θ_p, rad
1.57816	3.08090	-0.16040	-0.29679
1.63076	3.06767	-0.18551	-0.31022
1.68337	3.05574	-0.21098	-0.32450
1.73598	3.04507	-0.23672	-0.33954
1.78858	3.03566	-0.26266	-0.35522
1.84119	3.02756	-0.28873	-0.37148
1.89379	3.02072	-0.31487	-0.38824
1.94640	3.01517	-0.34105	-0.40546
1.99900	3.01092	-0.36720	-0.42309
2.05161	3.00797	-0.39330	-0.44112
2.05912	3.00766	-0.39702	-0.44372
2.06664	3.00736	-0.40074	-0.44633
2.07415	3.00710	-0.40446	-0.44895
2.08167	3.00688	-0.40817	-0.45157
2.08918	3.00667	-0.41188	-0.45421
2.09670	3.00648	-0.41560	-0.45685
2.10421	3.00633	-0.41931	-0.45951
2.11173	3.00621	-0.42301	-0.46216
2.11924	3.00612	-0.42672	-0.46482
2.12676	3.00605	-0.43042	-0.46749
2.13427	3.00601	-0.43412	-0.47017
2.14179	3.00602	-0.43781	-0.47286

34

TABLE X.—ROTOR II BLADE COORDINATES A SHROUD

X, in.	R, in.	Θ_s, rad	Θ_p, rad
0.26300	0.26300	-0.01665	-0.01665
0.26302	7.22880	-0.01577	-0.02094
0.26531	7.21328	-0.01106	-0.02125
0.27010	7.18097	-0.00622	-0.02326
0.27500	7.14882	-0.00273	-0.02404
0.27984	7.11682	-0.00012	-0.02427
0.28462	7.08492	0.00216	-0.02413
0.28938	7.05306	0.00412	-0.02372
0.29413	7.02121	0.00588	-0.02307
0.29889	6.98935	0.00740	-0.02223
0.30366	6.95743	0.00875	-0.02145
0.30844	6.92546	0.00996	-0.02074
0.31323	6.89335	0.01101	-0.02018
0.31805	6.86112	0.01192	-0.01985
0.32289	6.82874	0.01269	-0.01979
0.32777	6.79620	0.01336	-0.01999
0.33294	6.76358	0.01390	-0.02037
0.33854	6.73094	0.01433	-0.02086
0.34457	6.69832	0.01467	-0.02141
0.35104	6.66572	0.01491	-0.02199
0.35794	6.63317	0.01504	-0.02258
0.36529	6.60067	0.01506	-0.02320
0.37306	6.56826	0.01495	-0.02383
0.38126	6.53591	0.01474	-0.02447
0.38987	6.50366	0.01442	-0.02515
0.39889	6.47152	0.01397	-0.02587
0.40831	6.43951	0.01344	-0.02669
0.41813	6.40761	0.01288	-0.02757
0.42835	6.37585	0.01228	-0.02853
0.43895	6.34425	0.01156	-0.02956

TABLE X.—Continued.

X, in.	R, in.	Θ_s, rad	Θ_p, rad
0.44993	6.31279	0.01074	-0.03065
0.46128	6.28150	0.00981	-0.03183
0.47300	6.25038	0.00881	-0.03308
0.48509	6.21939	0.00769	-0.03441
0.49752	6.18862	0.00646	-0.03585
0.51029	6.15802	0.00511	-0.03737
0.52342	6.12760	0.00363	-0.03900
0.53683	6.09750	0.00207	-0.04071
0.55060	6.06751	0.00037	-0.04252
0.56469	6.03771	-0.00143	-0.04446
0.57909	6.00813	-0.00340	-0.04646
0.59381	5.97872	-0.00546	-0.04860
0.60883	5.92958	-0.00763	-0.05081
0.62413	5.92061	-0.00994	-0.05317
0.63973	5.89185	-0.01234	-0.05562
0.65562	5.86332	-0.01486	-0.05824
0.67179	5.83501	-0.01753	-0.06099
0.68823	5.80691	-0.02030	-0.06381
0.70494	5.77903	-0.23180	-0.06683
0.72192	5.75137	-0.02622	-0.06997
0.73916	5.72393	-0.02938	-0.07323
0.75665	5.69670	-0.03270	-0.07661
0.77440	5.66970	-0.03609	-0.08017
0.79238	5.64292	-0.03970	-0.08389
0.81062	5.61635	-0.04339	-0.08769
0.82909	5.59002	-0.04730	-0.09170
0.84780	5.56389	-0.05129	-0.09585
0.86674	5.53800	-0.05546	-0.10011
0.88590	5.51229	-0.05979	-0.10457
0.90530	5.48680	-0.06427	-0.10914

TABLE X.—Continued.

X, in.	R, in.	Θ_s, rad	Θ_p, rad
0.92492	5.46156	-0.06893	-0.11391
0.94475	5.43651	-0.07370	-0.11879
0.96481	5.41167	-0.07868	-0.12387
0.98508	5.38705	-0.08385	-0.12914
1.00557	5.36262	-0.08913	-0.13454
1.02627	5.33842	-0.09462	-0.14005
1.04718	5.31441	-0.10032	-0.14584
1.06831	5.29061	-0.10615	-0.15175
1.08963	5.26700	-0.11219	-0.15786
1.11118	5.24359	-0.11843	-0.16410
1.13293	5.22039	-0.12488	-0.17055
1.15489	5.19736	-0.13146	-0.17721
1.17707	5.17453	-0.13840	-0.18409
1.19946	5.15189	-0.14535	-0.19118
1.22206	5.12943	-0.15266	-0.19840
1.24487	5.10716	-0.16009	-0.20583
1.26791	5.08507	-0.16773	-0.21348
1.29118	5.06316	-0.17559	-0.22134
1.31467	5.04142	-0.18366	-0.22941
1.33841	5.01991	-0.19190	-0.23759
1.36238	4.99857	-0.20045	-0.24607
1.38662	4.97748	-0.20916	-0.25466
1.41110	4.95655	-0.21810	-0.26333
1.43586	4.93589	-0.22724	-0.27230
1.46088	4.91545	-0.23648	-0.28135
1.48621	4.89529	-0.24605	-0.29050
1.51181	4.87537	-0.25596	-0.29994
1.53772	4.85575	-0.26570	-0.30933
1.56395	4.83640	-0.27607	-0.31892
1.59051	4.81742	-0.28651	-0.32868

TABLE X.—Concluded.

X, in.	R, in.	Θ_s, rad	Θ_p, rad
1.61740	4.79873	-0.29728	-0.33839
1.64466	4.78063	-0.30817	-0.34839
1.67230	4.76313	-0.31940	-0.35834
1.70030	4.74617	-0.33097	-0.36857
1.72868	4.72989	-0.34263	-0.37874
1.75744	4.71428	-0.35464	-0.38917
1.78658	4.69920	-0.36697	-0.39941
1.81611	4.68457	-0.37938	-0.40991
1.84605	4.67036	-0.39211	-0.42056
1.87640	4.65654	-0.40542	-0.43122
1.90719	4.64306	-0.41880	-0.44202
1.38440	4.62992	-0.43221	-0.45341
1.94030	4.62920	-0.43301	-0.45409

TABLE XI.—ROTOR II: HOT SECTION II

X, in.	R, in.	Θ_s, rad	Θ_p, rad
0.13100	7.22950	-0.01667	-0.01667
0.13102	7.22850	-0.01579	-0.02097
0.13106	7.22688	-0.01446	-0.02178
0.13114	7.22359	-0.01339	-0.02233
0.13122	7.21994	-0.01246	-0.02275
0.13131	7.21607	-0.01162	-0.02308
0.13140	7.21204	-0.01084	-0.02334
0.13149	7.20786	-0.01011	-0.02356
0.13159	7.20360	-0.00941	-0.02374
0.13168	7.19925	-0.00875	-0.02389
0.13178	7.19483	-0.00811	-0.02401
0.13188	7.19036	-0.00749	-0.02410
0.13198	7.18582	-0.00689	-0.02418
0.13210	7.18124	-0.00632	-0-02424
0.13221	7.17662	-0.00575	-0.02428
0.13233	7.17194	-0.00521	-0.02430

TABLE XI.—Continued.

X, in.	R, in.	Θ_s, rad	Θ_p, rad
0.13245	7.16724	-0.00467	-0.02432
0.13257	7.16252	-0.00415	-0-02431
0.13269	7.15774	-0.00364	-0.02430
0.13281	7.15290	-0.00314	-0.02428
0.13356	7.13039	-0.00122	-0.02424
0.13451	7.10789	0.00051	-0.02420
0.13564	7.08537	0.00210	-0.02414
0.13695	7.06286	0.00356	-0.02408
0.13846	7.04036	0.00491	-0.02401
0.14014	7.01785	0.00617	-0.02393
0.14200	6.99533	0.00735	-0.02385
0.14403	6.97282	0.00845	-0.02375
0.14623	6.95032	0.00949	-0.02365
0.14861	6.92780	0.01047	-0.02354
0.15114	6.90529	0.01139	-0.02343
0.15385	6.88278	0.01226	-0.02331
0.15672	6.86027	0.01308	-0.02315
0.15975	6.83776	0.01386	-0.02305
0.16295	6.81525	0.01459	-0.02291
0.16629	6.79275	0.01529	-0.02276
0.16981	6.77023	0.01595	-0.02192
0.17347	6.74772	0.01657	-0.02130
0.17729	6.72521	0.01715	-0.02084
0.18127	6.70270	0.01771	-0.02049
0.18940	6.68019	0.01823	-0.02025
0.18968	6.65768	0.01872	-0.02010
0.19412	6.63517	0.01918	-0.02003
0.19870	6.61266	0.01961	-0.02005
0.20344	6.59015	0.02001	-0.02014
0.20832	6.56764	0.02039	-0.02031
0.21336	6.54513	0.02074	-0.02056
0.21853	6.52262	0.02106	-0.02090
0.22389	6.50000	0.02136	-0.02134
0.24932	6.40001	0.02281	-0.02277
0.26310	6.34996	0.02341	-0.02374
0.28310	6.26168	0.02435	-0.02537
0.31310	6.18679	0.02510	-0.02784
0.34300	6.09918	0.02516	-0.03043

TABLE XI.—Continued.

X, in.	R, in.	Θ_s, rad	Θ_p, rad
0.37300	6.01744	0.02462	-0.03319
0.40300	5.94058	0.02355	-0.03614
0.43300	5.86788	0.02199	-0.03935
0.46300	5.79884	0.01997	-0.04277
0.49300	5.73299	0.01751	-0.04643
0.52300	5.67002	0.01465	-0.05033
0.55300	5.60966	0.01139	-0.05449
0.58300	5.55165	0.00775	-0.05887
0.61300	5.49583	0.00375	-0.06350
0.64300	5.44202	-0.00061	-0.06837
0.67300	5.39011	-0.00332	-0.07347
0.70300	5.33996	-0.01035	-0.07880
0.73300	5.29148	-0.01572	-0.08437
0.76300	5.24456	-0.02141	-0.09016
0.79300	5.19915	-0.02741	-0.09619
0.82300	5.15515	-0.03371	-0.10244
0.85300	5.11252	-0.04032	-0.10891
0.88300	5.07120	-0.04721	-0.11562
0.91300	5.03113	-0.05439	-0.12255
0.94300	4.99230	-0.06185	-0.12972
0.97300	4.95463	-0.06959	-0.13711
1.00300	4.91811	-0.07759	-0.14473
1.03300	4.88270	-0.08585	-0.15260
1.06300	4.84836	-0.09437	-0.16070
1.09300	4.81507	-0.10314	-0.16703
1.12300	4.78283	-0.11217	-0.17761
1.15300	4.75160	-0.12144	-0.18642
1.18300	4.72136	-0.13100	-0.19548
1.21300	4.69213	-0.14077	-0.20477
1.24300	4.66382	-0.15077	-0.21429
1.27300	4.63649	-0.16101	-0.22403
1.30300	4.61009	-0.17146	-0.23395
1.33300	4.58463	-0.18212	-0.24407
1.36300	4.56011	-0.19297	-0.25433
1.39300	4.53650	-0.20401	-0.26471
1.42300	4.51381	-0.21522	-0.27520
1.45300	4.49202	-0.22662	-0.28576
1.48300	4.47115	-0.23817	-0.29637

TABLE XI.—Concluded.

X, in.	R, in.	Θ_s, rad	Θ_p, rad
1.51300	4.45119	-0.24989	-0.30700
1.54300	4.43215	-0.26175	-0.31765
1.57300	4.41401	-0.27378	-0.32829
1.60300	4.39680	-0.28595	-0.33892
1.63300	4.38051	-0.29827	-0.34951
1.66300	4.36515	-0.31072	-0.36006
1.69300	4.36072	-0.32330	-0.37057
1.72300	4.35724	-0.33602	-0.38104
1.75300	4.32473	-0.34885	-0.39145
1.78300	4.31319	-0.36179	-0.40182
1.81300	4.30263	-0.37483	-0.41213
1.84300	4.29308	-0.38798	-0.42240
1.87300	4.28456	-0.40121	-0.43262
1.90300	4.27707	-0.41452	-0.44281
1.93300	4.27066	-0.42792	-0.45295
1.96300	4.26534	-0.44137	-0.46306

TABLE XII.—ROTOR II: HOT SECTION III

X, in.	R, in.	Θ_p, rad	Θ_s, rad
0.0	7.22950	-0.01667	-0.01667
0.00002	7.22580	-0.01579	-0.02097
0.00007	7.22688	-0.01446	-0.02178
0.00015	7.22359	-0.01340	-0.02233
0.00024	7.21994	-0.01247	-0.02275
0.00034	7.21607	-0.01162	-0.02308
0.00044	7.21204	-0.01084	-0.02335
0.00054	7.20784	-0.01011	-0.02356
0.00065	7.20360	-0.00941	-0.02374
0.00076	7.19925	-0.00875	-0.02389
0.00087	7.19483	-0.00611	-0.02401
0.00098	7.19036	-0.00749	-0-02411
0.00111	7.18582	-0.00690	-0.02418
0.00125	7.18124	-0.00632	-0.02424
0.00139	7.17661	-0.00576	-0.02428
0.00154	7.17194	-0.00521	-0.02431
0.00168	7.16725	-0.00467	-0.02432
0.00182	7.16252	-0.00415	-0.02432

TABLE XII.—Continued.

X, in.	R, in.	Θ_p, rad	Θ_s, rad
0.00197	7.15774	-0.00364	-0.02430
0.00214	7.15290	-0.00314	-0.02428
0.00293	7.13039	-0.00122	-0.02425
0.00382	7.10789	0.00051	-0.02420
0.00477	7.08537	0.00209	-0.02415
0.00581	7.06285	0.00355	-0.02409
0.00693	7.04036	0.00491	-0.02401
0.00813	7.01785	0.00617	-0.02394
0.00942	6.99534	0.00734	-0.02385
0.01078	6.97282	0.00845	-0.02376
0.01222	6.95032	0.00948	-0.02365
0.01375	6.92780	0.01046	-0-02355
0.01536	6.90529	0.01138	-0.02343
0.01706	6.88278	0.01225	-0.02331
0.01884	6.86027	0.01308	-0.02319
0.02070	6.83776	0.01385	-0.02305
0.02265	6.81525	0.01459	-0-02291
0.02468	6.79275	0.01529	-0.02277
0.02680	6.77023	0.01594	-0.02193
0.02901	6.74772	0.01656	-0.02130
0.03130	6.72521	0.01715	-0.02084
0.03368	6.70270	0.01771	-0.02050
0.03615	6.68019	0.01823	-0.02025
0.03870	6.65768	0.01872	-0.02010
0.04135	6.63517	0.01918	-0.02004
0.04408	6.61266	0.01961	-0.02005
0.04690	6.59015	0.02001	-0.02014
0.04981	6.56765	0.02039	-0.02031
0.05282	6.54513	0.02073	-0.02056
0.05592	6.52262	0.02106	-0.02090
0.05912	6.50000	0.02135	-0.02134
0.07442	6.40000	0.02280	-0.02278
0.09162	6.30000	0.02438	-0.02436
0.11078	6.20001	0.02611	-0.02610
0.13199	6.10000	0.02802	-0.02801
0.15534	6.00000	0.03008	-0.03007
0.18092	5.90000	0.03232	-0.03230
0.20885	5.80000	0.03478	-0.03477

TABLE XII.—Continued.

X, in.	R, in.	Θ_p, rad	Θ_s, rad
0.23925	5.70000	0.03747	-0.03745
0.26310	5.62709	0.03941	-0.03973
0.28310	5.56904	0.04103	-0.04205
0.31310	5.48675	0.04276	-0.04550
0.34300	5.40957	0.04371	-0.04899
0.37300	5.33684	0.04396	-0.05253
0.40300	5.26813	0.04356	-0.05617
0.43300	5.20298	0.04255	-0.05991
0.46300	5.14107	0.04096	-0.06377
0.49300	5.08213	0.03884	-0.06776
0.52300	5.02592	0.03621	-0.07190
0.55300	4.97222	0.03310	-0.07620
0.58300	4.92087	0.02952	-0.08065
0.61300	4.87169	0.02551	-0.08526
0.64300	4.82454	0.02106	-0.09005
0.67300	4.77930	0.01622	-0.09500
0.70300	4.73589	0.01098	-0.10014
0.73300	4.69419	0.00537	-0.10546
0.76300	4.65411	-0.00061	-0.11096
0.79300	4.61557	-0.00694	-0.11666
0.82300	4.57851	-0.01361	-0.12255
0.85300	4.54286	-0.02060	-0.12864
0.88300	4.50853	-0.02791	-0.13493
0.91300	4.47552	-0.03553	-0.14142
0.94300	4.44373	-0.04345	-0.14812
0.97300	4.41315	-0.05166	-0.15604
1.00300	4.38371	-0.06014	-0.16219
1.03300	4.35539	-0.06890	-0.16955
1.06300	4.32814	-0.07793	-0.17714
1.09300	4.30194	-0.08721	-0.18497
1.12300	4.27674	-0.09674	-0.19303
1.15300	4.25252	-0.10652	-0.20134
1.18300	4.22925	-0.11658	-0.20990
1.21300	4.20692	-0.12686	-0.21869
1.24300	4.18548	-0.13736	-0.22771
1.27300	4.16491	-0.14809	-0.23694
1.30300	4.14522	-0.15904	-0.24637
1.33300	4.12634	-0.17020	-0.25599

TABLE XII.—Concluded.

X, in.	R, in.	Θ_p, rad	Θ_s, rad
1.36300	4.10829	-0.18155	-0.26574
1.39300	4.09105	-0.19310	-0.27562
1.42300	4.07459	-0.20483	-0.28559
1.45300	4.05889	-0.21674	-0.29564
1.48300	4.04395	-0.22883	-0.30571
1.51300	4.02975	-0.24107	-0.31582
1.54300	4.01628	-0.25350	-0.32591
1.57300	4.00351	-0.26607	-0.33600
1.60300	3.99145	-0.27879	-0.34608
1.63300	3.98008	-0.29166	-0.35612
1.66300	3.96939	-0.30466	-0.36613
1.69300	3.95936	-0.31777	-0.37611
1.72300	3.95000	-0.33099	-0.38607
1.75300	3.94130	-0.34431	-0.39599
1.78300	3.93322	-0.35770	-0.40590
1.81300	3.92578	-0.37119	-0.41578
1.84300	3.91897	-0.38472	-0.42566
1.87300	3.91277	-0.39831	-0.43553
1.78300	3.93322	-0.35770	-0.40590
1.81300	3.92578	-0.37119	-0.41578
1.84300	3.91897	-0.38472	-0.42566
1.87300	3.91277	-0.39831	-0.43553
1.90300	3.90720	-0.41194	-0.44539
1.93300	3.90222	-0.42560	-0.45527
1.96300	3.89785	-0.43929	-0.46514
1.98200	3.89544	-0.44797	-0.47140

TABLE XIII.—ROTOR II: HOT SECTION IV

X, in.	R, in.	Θ_s, rad	Θ_p, rad
-0.13150	7.22950	-0.01668	-0.01668
-0.13149	7.22880	-0.01580	-0.02093
-0.13148	7.22688	-0.01446	-0.02178
-0.13146	7.22359	-0.01340	-0.02234
-0.13143	7.21994	-0.01247	-0.02275
-0.13140	7.21607	-0.01163	-0.02308
-0.13137	7.21204	-0.01094	-0.02335
-0.13134	7.20784	-0.01011	-0.02356

TABLE XIII.—Continued.

X, in.	R, in.	Θ_s, rad	Θ_p, rad
-0.13131	7.20360	-0.00941	-0.02374
-0.13127	7.19925	-0.00875	-0.02389
-0.13124	7.19483	-0.00811	-0.02401
-0.13121	7.19036	-0.00749	-0.02411
-0.13117	7.18582	-0.00690	-0.02418
-0.13114	7.18124	-0.00632	-0.02424
-0.13110	7.17661	-0.00576	-0.02428
-0.13107	7.17195	-0.00521	-0.02431
-0.13103	7.16724	-0.00467	-0.02432
-0.13100	7.16253	-0.00415	-0.02432
-0.13096	7.15774	-0.00364	-0.02431
-0.13092	7.15290	-0.00315	-0.02428
-0.13075	7.13039	-0.00123	-0.02425
-0.13058	7.10789	0.00051	-0.02420
-0.13030	7.08537	0.00209	-0.02415
-0.12989	7.06285	0.00355	-0.02409
-0.12947	7.04036	0.00490	-0.02402
-0.12894	7.01785	0.00616	-0.02394
-0.12839	6.99534	0.00734	-0.02385
-0.12775	6.97282	0.00845	-0.02376
-0.12706	6.95032	0.00948	-0.02366
-0.12632	6.92780	0.01046	-0.02355
-0.12551	6.90529	0.01138	-0.02343
-0.12464	6.88278	0.01225	-0.02331
-0.12370	6.86027	0.01308	-0.02319
-0.12271	6.83776	0.01385	-0.02305
-0.13165	6.81535	0.01459	-0.02291
-0.12054	6.79275	0.01528	-0.02277
-0.11936	6.77023	0.01594	-0.02193
-0.11811	6.74772	0.01656	-0.02131
-0.11680	6.72521	0.01715	-0.02084
-0.11543	6.70270	0.01770	-0.02050
-0.11399	6.68019	0.01822	-0.02026
-0.11250	6.65768	0.01871	-0.02010
-0.11093	6.63517	0.01917	-0.02004
-0.10930	6.61266	0.01961	-0.02005
-0.10760	6.59015	0.02001	-0.02014
-0.10583	6.56765	0.02038	-0.02031

TABLE XIII.—Continued.

X, in.	R, in.	Θ_s, rad	Θ_p, rad
-0.10400	6.54513	0.02073	-0.02057
-0.10210	6.52261	0.02105	-0.02091
-0.10012	6.50000	0.02135	-0.02134
-0.09054	6.40000	0.02279	-0.02279
-0.07956	6.30000	0.02437	-0.02437
-0.06713	6.20000	0.02611	-0.02610
-0.05318	6.10000	0.02802	-0.02801
-0.03766	6.00000	0.03008	-0.03007
-0.02051	5.90000	0.03232	-0.03231
-0.00163	5.80000	0.03478	-0.03477
0.01904	5.70000	0.03747	-0.03746
0.04160	5.60000	0.04039	-0.04038
0.06617	5.50000	0.04355	-0.04354
0.09284	5.40000	0.04703	-0.04702
0.12177	5.30000	0.05078	-0.05077
0.15309	5.20000	0.05487	-0.05486
0.16970	5.15001	0.05703	-0.05701
0.17242	5.14200	0.05738	-0.05736
0.19716	5.07144	0.06062	-0.06060
0.22630	4.99302	0.06444	-0.06442
0.25619	4.91735	0.06835	-0.06830
0.26310	4.90056	0.06908	-0.06941
0.28310	4.85296	0.07133	-0.07234
0.31310	4.78479	0.07371	-0.07645
0.34300	4.72015	0.07505	-0.08033
0.37300	4.65877	0.07551	-0.08408
0.40300	4.60035	0.07517	-0.08778
0.43300	4.54468	0.07413	-0.09149
0.46300	4.49155	0.07245	-0.09525
0.49300	4.44080	0.07018	-0.09910
0.52300	4.39226	0.06737	-0.10306
0.55300	4.34580	0.06406	-0.10715
0.58300	4.30129	0.06026	-0.11138
0.61300	4.25864	0.05602	-0.11578
0.64300	4.21774	0.05135	-0.12033
0.67300	4.17849	0.04628	-0.12507
0.70300	4.14084	0.04082	-0.12998
0.73300	4.10468	0.03499	-0.13508

TABLE XIII.—Continued.

X, in.	R, in.	Θ_s, rad	Θ_p, rad
0.76300	4.06997	0.02879	-0.14036
0.79300	4.03662	0.02224	-0.14584
0.82300	4.00460	0.01535	-0.15150
0.85300	3.97386	0.00813	-0.15736
0.88300	3.94431	0.00058	-0.16341
0.91300	3.91595	-0.00729	-0.16966
0.94300	3.88870	-0.01547	-0.17610
0.97300	3.86255	-0.02397	-0.18273
1.00300	3.83746	-0.03277	-0.18955
1.03300	3.81339	-0.04187	-0.19658
1.06300	3.79031	-0.05128	-0.20378
1.09300	3.76818	-0.06099	-0.21116
1.12300	3.74698	-0.07099	-0.21878
1.15300	3.72668	-0.08129	-0.22657
1.18300	3.70728	-0.09190	-0.23459
1.21300	3.68871	-0.10276	-0.24278
1.24300	3.67098	-0.11389	-0.25117
1.27300	3.65407	-0.12528	-0.25975
1.30300	3.63794	-0.13692	-0.26849
1.33300	3.62261	-0.14880	-0.27738
1.36300	3.60800	-0.16091	-0.28638
1.39300	3.59414	-0.17325	-0.29547
1.42300	3.58103	-0.18578	-0.30463
1.45300	3.56859	-0.19853	-0.31384
1.48300	3.55686	-0.21147	-0.32307
1.51300	3.54580	-0.22462	-0.33227
1.54300	3.53543	-0.23792	-0.34148
1.57300	3.52568	-0.25141	-0.35067
1.60300	3.51660	-0.26506	-0.35981
1.63300	3.50813	-0.27883	-0.36895
1.66300	3.50029	-0.29274	-0.37804
1.69300	3.49305	-0.30475	-0.38713
1.72300	3.48641	-0.32094	-0.39621
1.75300	3.48036	-0.33502	-0.40527
1.78300	3.47489	-0.34928	-0.41433
1.81300	3.46999	-0.36356	-0.42341
1.84300	3.46566	-0.37789	-0.43248
1.87300	3.46187	-0.39225	-0.44158

TABLE XIII.—Concluded.

X, in.	R, in.	Θ_s, rad	Θ_p, rad
1.90300	3.45863	-0.40662	-0.45072
1.93300	3.45593	-0.42099	-0.45988
1.96300	3.45377	-0.43534	-0.46908
1.99300	3.45212	-0.44971	-0.47832
2.00300	3.45174	-0.45448	-0.48142

TABLE XIV.—ROTOR II BLADE COORDINATES AT HUB

X, in.	R, in.	Θ_s, rad	Θ_p, rad
-0.26300	7.22950	-0.01668	-0.01668
-0.26300	7.22880	-0.01580	-0.02098
-0.26300	7.22688	-0.01446	-0.02179
-0.26300	7.22359	-0.01340	-0.02234
-0.26300	7.21995	-0.01247	-0.02275
-0.26300	7.21607	-0.01163	-0.02308
-0.26300	7.21204	-0.01085	-0.02335
-0.26300	7.20786	-0.01011	-0.02357
-0.26300	7.20360	-0.00942	-0.02375
-0.26300	7.19925	-0.00875	-0.02389
-0.26300	7.19483	-0.00811	-0.02401
-0.26300	7.19036	-0.00750	-0.02411
-0.26300	7.18582	-0.00690	-0.02419
-0.26300	7.18124	-0.00632	-0.02424
-0.26300	7.17661	-0.00572	-0.02428
-0.26300	7.17194	-0.00521	-0.02431
-0.26300	7.16725	-0.00468	-0.02432
-0.26300	7.16252	-0.00415	-0.02432
-0.26300	7.19925	-0.00875	-0.02389
-0.26300	7.19483	-0.00811	-0.02401
-0.26300	7.19036	-0.00750	-0.02411
-0.26300	7.18582	-0.00690	-0.02419
-0.26300	7.18124	-0.00632	-0.02424
-0.26300	7.17661	-0.00572	-0.02428

TABLE XIV.—Continued.

X, in.	R, in.	Θ_s, rad	Θ_p, rad
-0.26300	7.17194	-0.00521	-0.02431
-0.26300	7.16725	-0.00468	-0.02432
-0.26300	7.16252	-0.00415	-0.02432
-0.26300	7.15774	-0.00364	-0.02431
-0.26300	7.15290	-0.00315	-0.02428
-0.26300	7.13039	-0.00123	-0.02425
-0.26300	7.10789	0.00051	-0.02421
-0.26300	7.08537	0.00209	-0.02415
-0.26300	7.06286	0.00355	-0.02409
-0.26300	7.04036	0.00490	-0.02402
-0.26300	7.01785	0.00616	-0.02394
-0.26300	6.99533	0.00734	-0.02385
-0.26300	6.97282	0.00844	-0.02376
-0.26300	6.95032	0.00948	-0.02366
-0.26300	6.92780	0.01046	-0.02355
-0.26300	6.90529	0.01138	-0.02344
-0.26300	6.88278	0.01225	-0.02332
-0.26300	6.86027	0.01307	-0.02319
-0.26300	6.83776	0.01385	-0.02306
-0.26300	6.81526	0.01459	-0.02292
-0.26300	6.79275	0.01528	-0.02277
-0.26300	6.77023	0.01594	-0.02193
-0.26300	6.74771	0.01656	-0.02131
-0.26300	6.72521	0.01715	-0.02084
-0.26300	6.70270	0.01770	-0.02050
-0.26300	6.68019	0.01822	-0.02026
-0.26300	6.65768	0.01871	-0.02011
-0.26300	6.63517	0.01917	-0.02004
-0.26300	6.61266	0.01960	-0.02005
-0.26300	6.59015	0.02001	-0.02015

TABLE XIV.—Continued.

X, in.	R, in.	Θ_s, rad	Θ_p, rad
-0.26300	6.56765	0.02038	-0.02032
-0.26300	6.54513	0.02073	-0.02057
-0.26300	6.52263	0.02105	-0.02091
-0.26300	6.50000	0.02135	-0.02135
-0.26300	6.40000	0.02279	-0.02279
-0.26300	6.30000	0.02437	-0.02437
-0.26300	6.20000	0.02611	-0.02611
-0.26300	6.10000	0.02801	-0.02801
-0.26300	6.00000	0.03008	-0.03008
-0.26300	5.90000	0.03231	-0.03231
-0.26300	5.80000	0.03477	-0.03477
-0.26300	5.70000	0.03746	-0.03746
-0.26300	5.60000	0.04039	-0.04039
-0.26300	5.50000	0.04355	-0.04355
-0.26300	5.40000	0.04703	-0.04703
-0.26300	5.30000	0.05077	-0.05077
-0.26300	5.20000	0.05487	-0.05487
-0.26300	5.15000	0.05702	-0.05702
-0.26300	5.14200	0.05737	-0.05737
-0.23691	5.07143	0.06061	-0.06061
-0.20691	4.99302	0.06443	-0.06443
-0.17961	4.91735	0.06832	-0.06832
-0.14692	4.84430	0.07233	-0.07233
-0.11692	4.77378	0.07639	-0.07639
-0.08692	4.70565	0.08051	-0.08051
-0.05692	4.63981	0.08473	-0.08472
-0.02692	4.57617	0.08896	-0.08896
0.00307	4.51466	0.09324	-0.09323
0.03307	4.45517	0.09756	-0.09755
0.06307	4.39765	0.10190	-0.10189

TABLE XIV.—Continued.

X, in.	R, in.	Θ_s, rad	Θ_p, rad
0.09307	4.34198	0.10723	-0.10721
0.12307	4.28814	0.11110	-0.11109
0.15306	4.23606	0.11480	-0.11479
0.18306	4.18563	0.11843	-0.11842
0.21306	4.13685	0.12202	-0.12200
0.24306	4.08963	0.12557	-0.12555
0.26310	4.05900	0.12795	-0.12828
0.28310	4.02905	0.13005	-0.13107
0.31310	3.98528	0.13221	-0.13496
0.34300	3.94296	0.13330	-0.13858
0.37300	3.90200	0.13345	-0.14202
0.40300	3.86234	0.13274	-0.14535
0.43300	3.82398	0.13126	-0.14862
0.46300	3.78687	0.12908	-0.15188
0.49300	3.75096	0.12625	-0.15517
0.52300	3.71624	0.12282	-0.15852
0.55300	3.68166	0.11885	-0.16195
0.58300	3.65019	0.11437	-0.16550
0.61300	3.61880	0.10942	-0.16917
0.64300	3.58848	0.10402	-0.17300
0.67300	3.55917	0.09821	-0.17700
0.70300	3.53088	0.09201	-0.18117
0.73300	3.50356	0.08545	-0.18554
0.76300	3.47718	0.07855	-0.19012
0.79300	3.45174	0.07131	-0.19491
0.82300	3.42719	0.06378	-0.19993
0.85300	3.40353	0.05594	-0.20518
0.88300	3.38074	0.04778	-0.21062
0.91300	3.35880	0.03930	-0.21625
0.94300	3.33767	0.03050	-0.22207

51

TABLE XIV.—Continued.

X, in.	R, in.	Θ_s, rad	Θ_p, rad
0.97300	3.31735	0.02137	-0.22807
1.00300	3.29782	0.01191	-0.23424
1.03300	3.27906	0.00213	-0.24058
1.06300	3.26105	-0.00799	-0.24709
1.09300	3.24378	-0.01844	-0.25374
1.12300	3.22723	-0.02923	-0.26055
1.15300	3.21140	-0.04036	-0.26750
1.18300	3.19624	-0.05188	-0.27461
1.21300	3.18177	-0.06372	-0.28183
1.24300	3.16798	-0.07591	-0.28916
1.27300	3.15483	-0.08845	-0.29659
1.30300	3.14230	-0.10133	-0.30408
1.33300	3.13041	-0.11456	-0.31163
1.36300	3.11913	-0.12810	-0.31920
1.39300	3.10846	-0.01419	-0.32679
1.42300	3.09838	-0.15604	-0.33438
1.45300	3.08887	-0.17039	-0.34198
1.48300	3.07994	-0.18496	-0.34958
1.51300	3.07157	-0.19970	-0.35719
1.54300	3.06375	-0.21460	-0.36480
1.57300	3.05647	-0.22965	-0.37243
1.60300	3.04972	-0.24480	-0.38006
1.63300	3.04348	-0.26006	-0.38773
1.66300	3.03775	-0.27537	-0.39541
1.69300	3.03253	-0.29075	-0.40313
1.72300	3.02781	-0.30617	-0.41088
1.75300	3.02357	-0.32163	-0.41867
1.78300	3.01981	-0.33710	-0.42650
1.81300	3.01651	-0.35259	-0.43438
1.84300	3.01368	-0.36807	-0.44231

TABLE XIV.—Concluded.

X, in.	R, in.	Θ_s, rad	Θ_p, rad
1.87300	3.01130	-0.38354	-0.45029
1.90300	3.00938	-0.39901	-0.45833
1.93300	3.00789	-0.41445	-0.46642
1.96300	3.00683	-0.42986	-0.47458
1.99300	3.00621	-0.44523	-0.48279
2.02300	3.00600	-0.46057	-0.49108

Appendix B

Rotor Exit Surveys
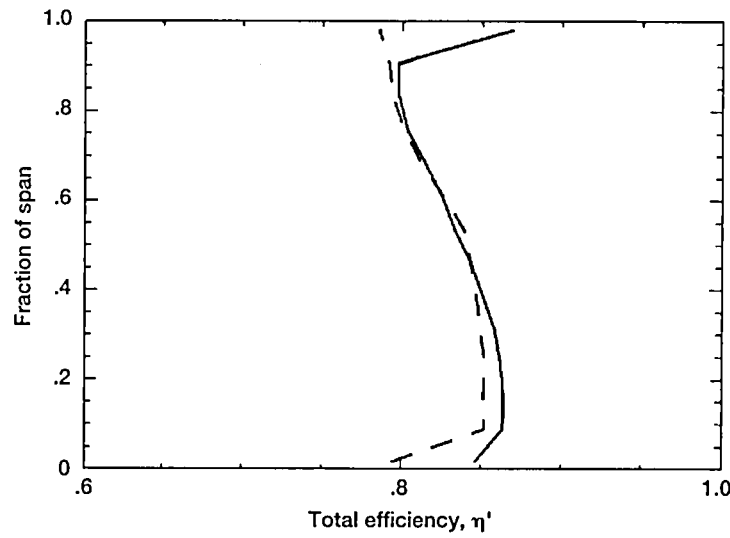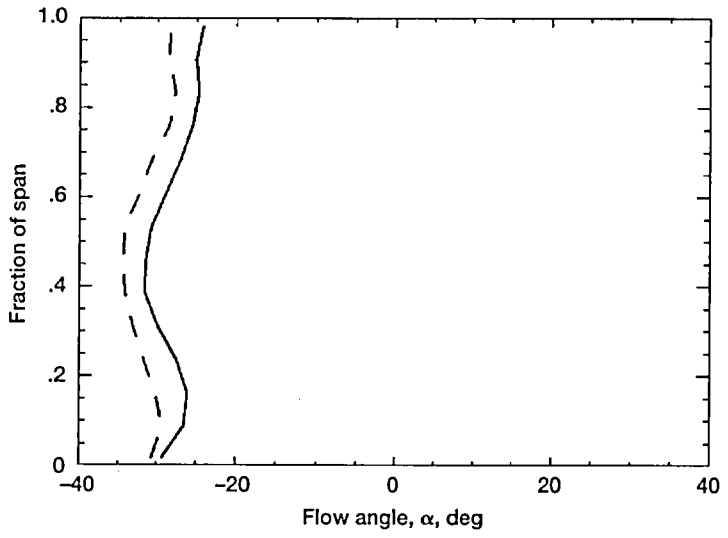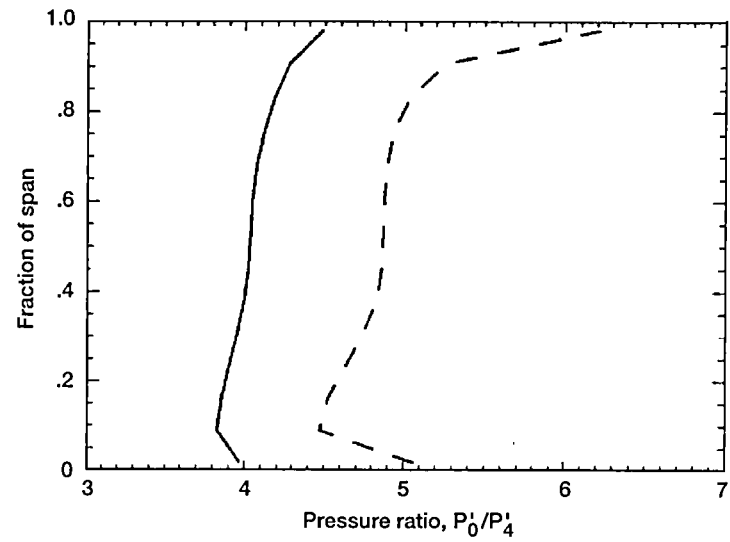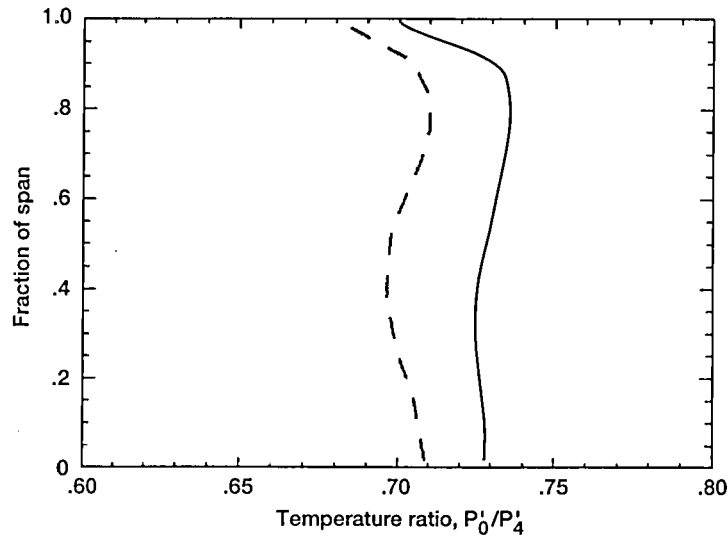
Figure 36.—Turbine exit radial surveys at 80 percent of design speed for rotor I-stator I configuration at various pressure ratios.
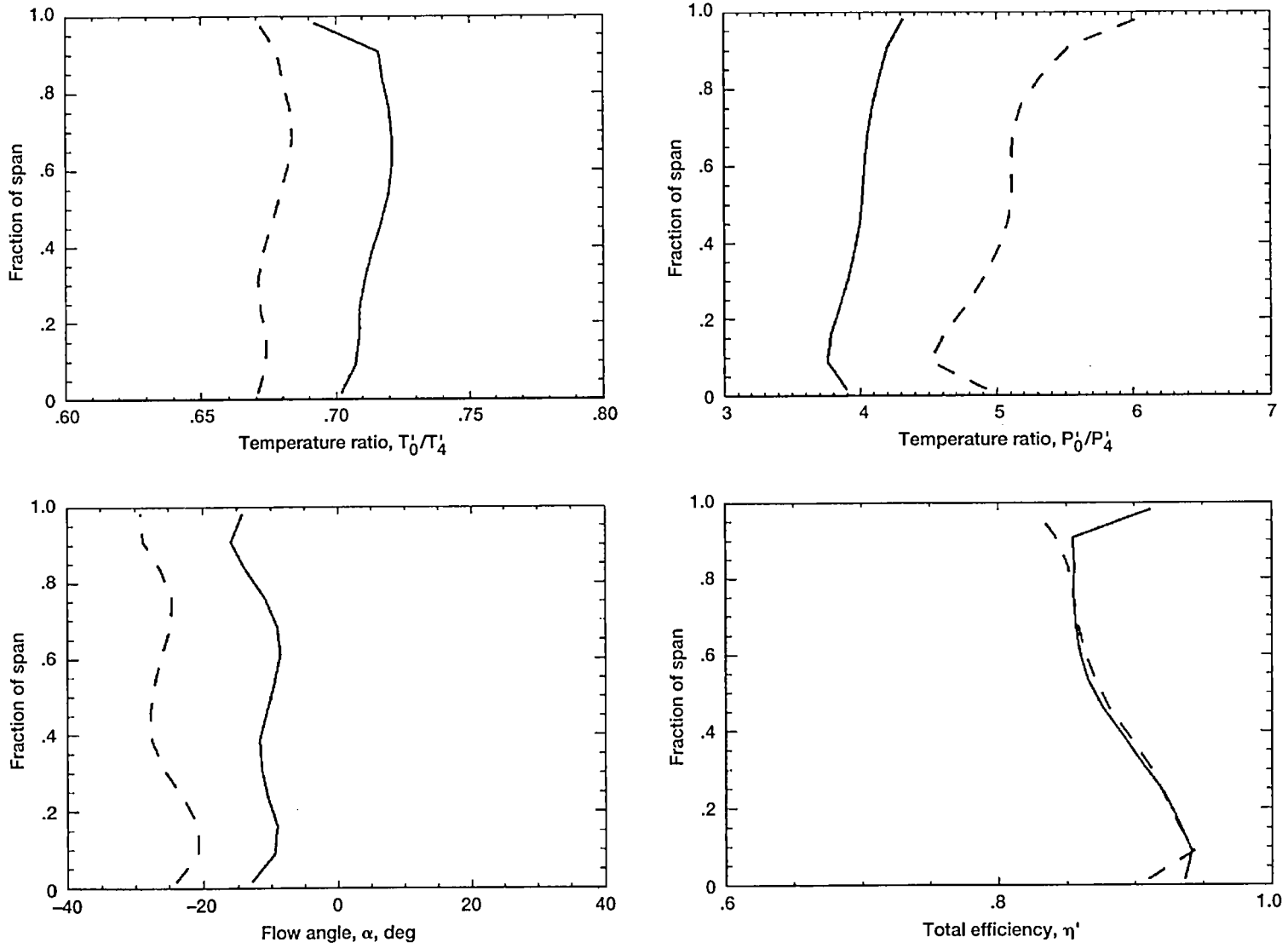
Figure 37.—Turbine exit radial surveys at 100 percent of design speed for rotor I-stator I configuration at various pressure ratios.
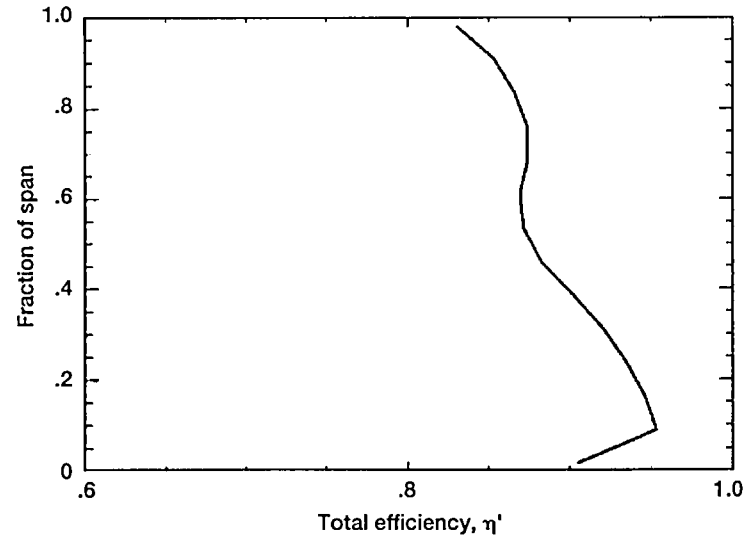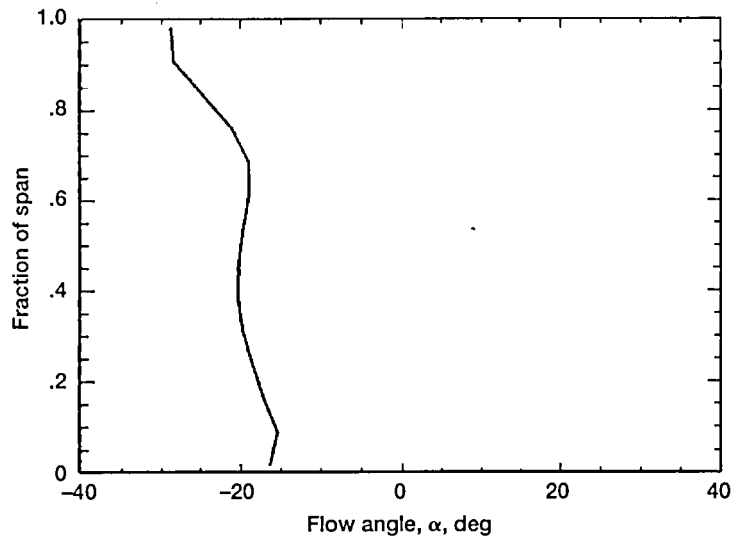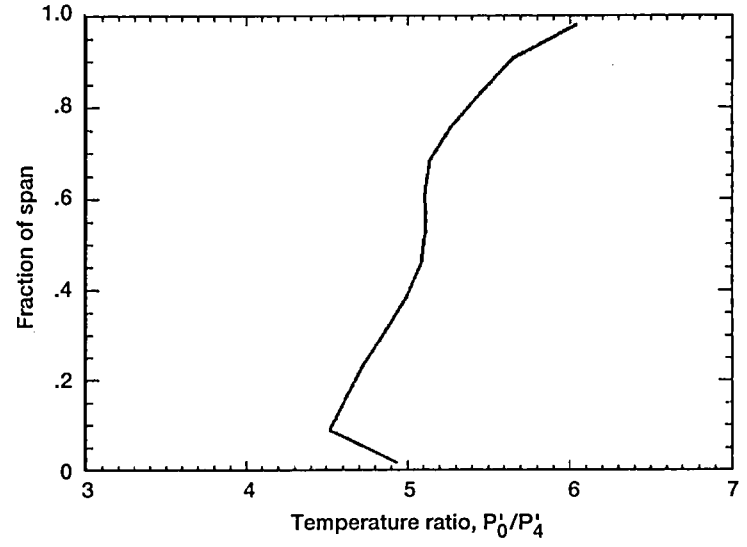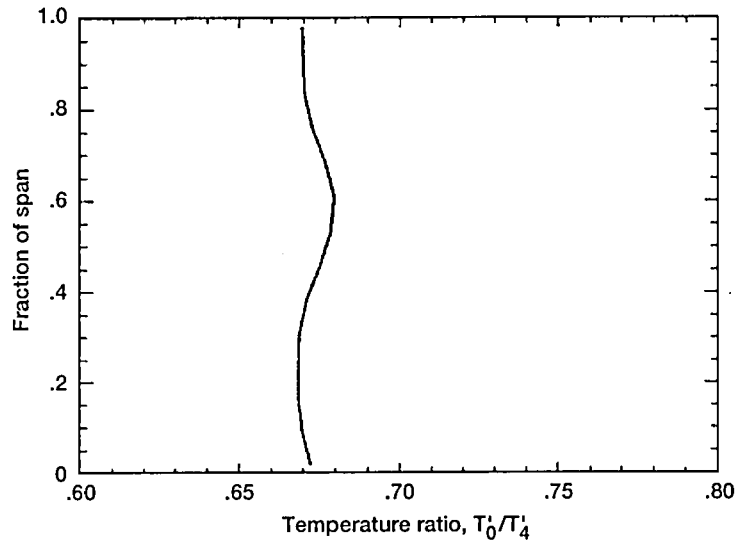
Figure 38.—Turbine exit radial surveys at 110 percent of design speed for rotor I-stator I configuration at design pressure ratio.
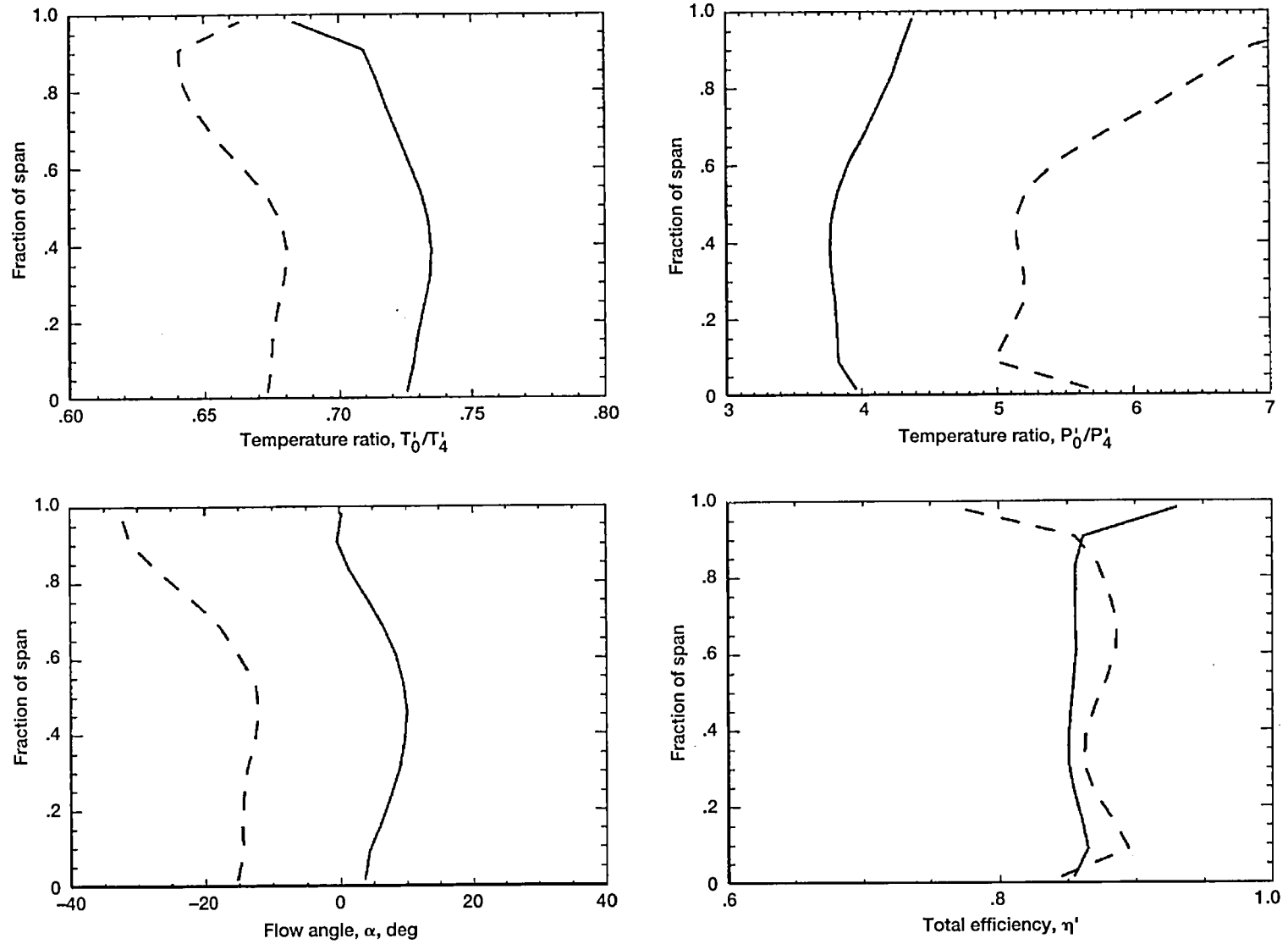
Figure 39.—Turbine exit radial surveys at 120 percent of design speed for rotor I-stator I configuration at various pressure ratios.
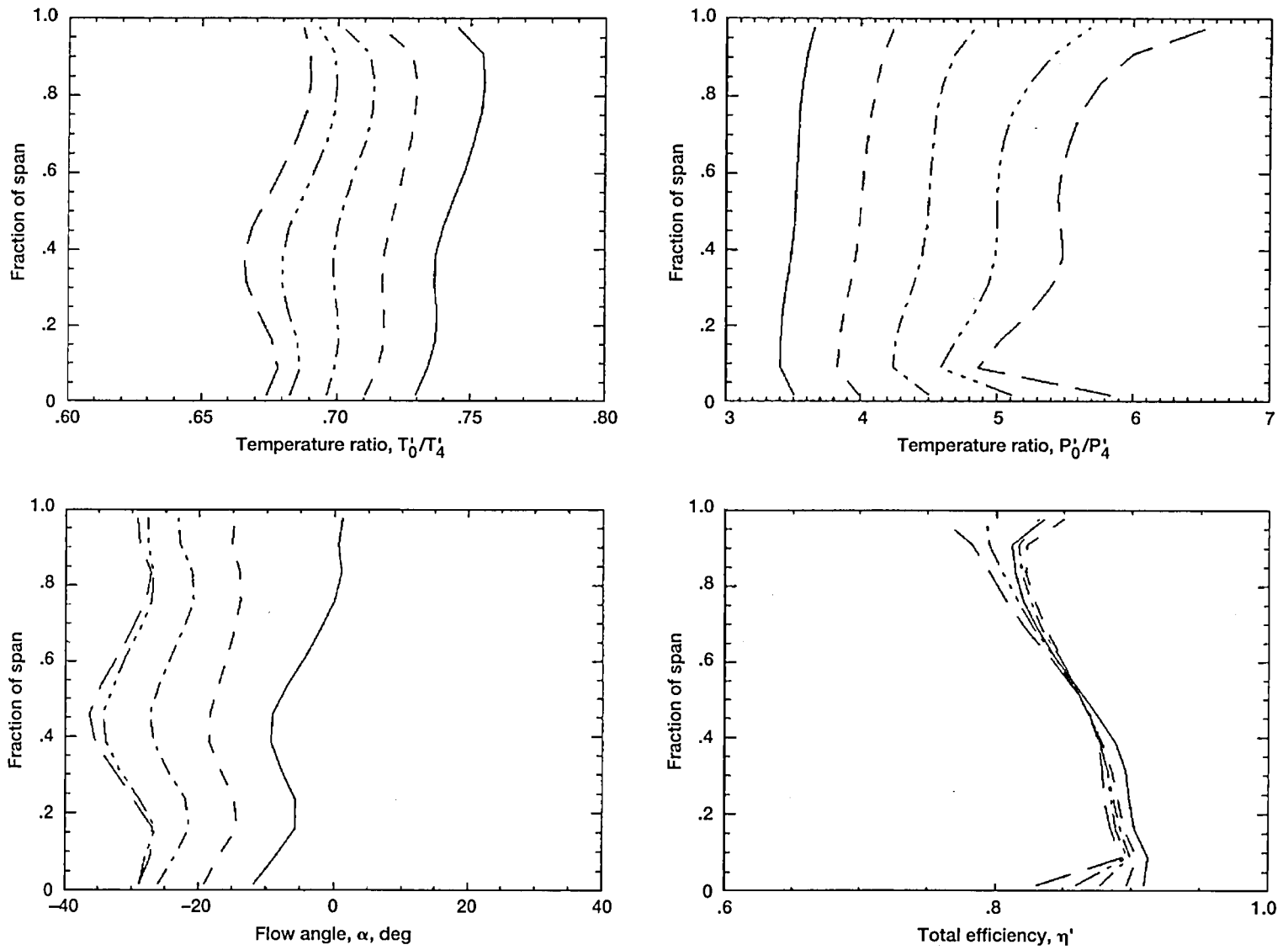
Figure 40.—Turbine exit radial surveys at 90 percent of design speed for rotor I-stator II configuration at various pressure ratios.
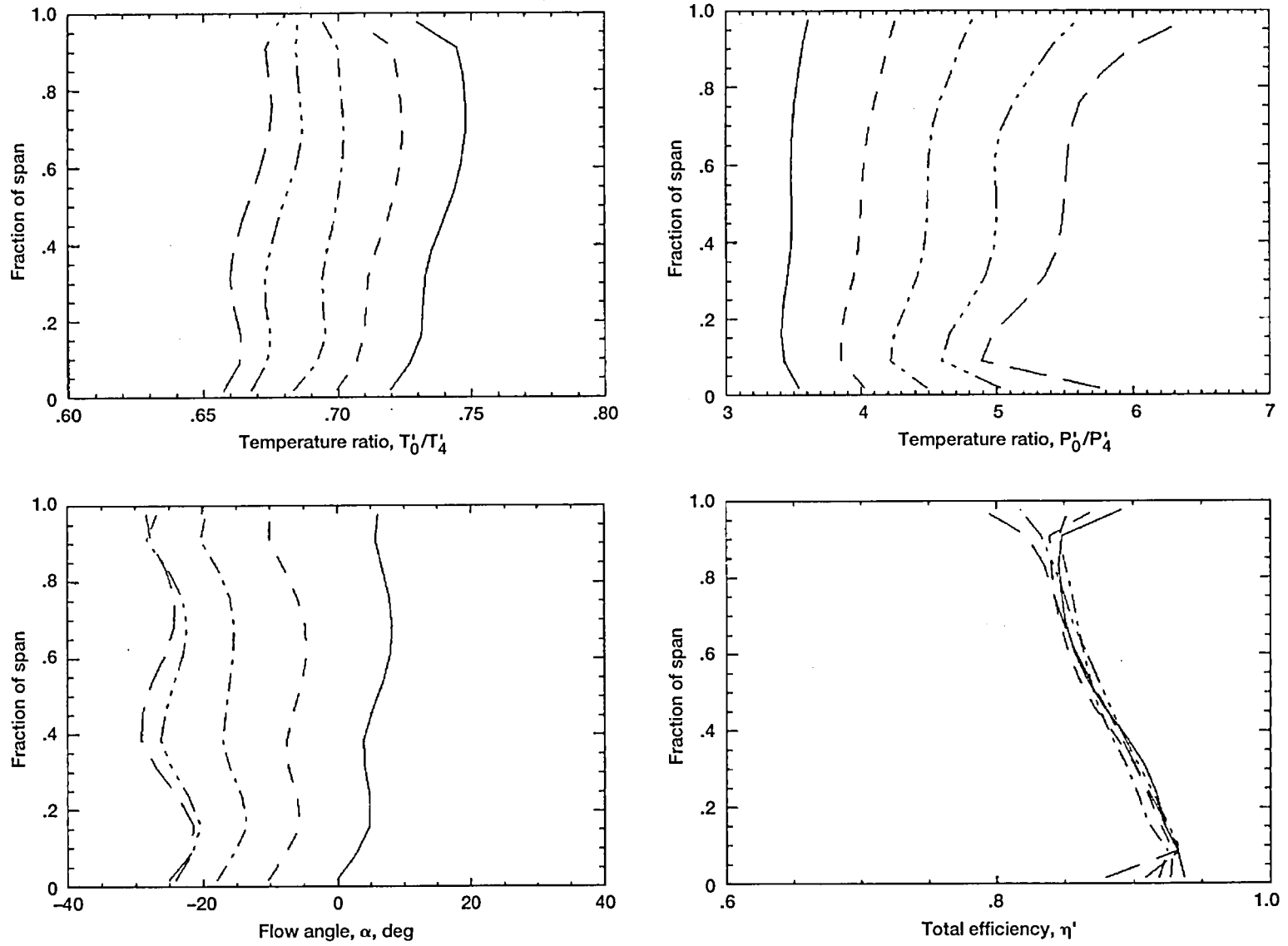
Figure 41.—Turbine exit radial surveys at 100 percent of design speed for rotor I-stator II configuration at various pressure ratios.
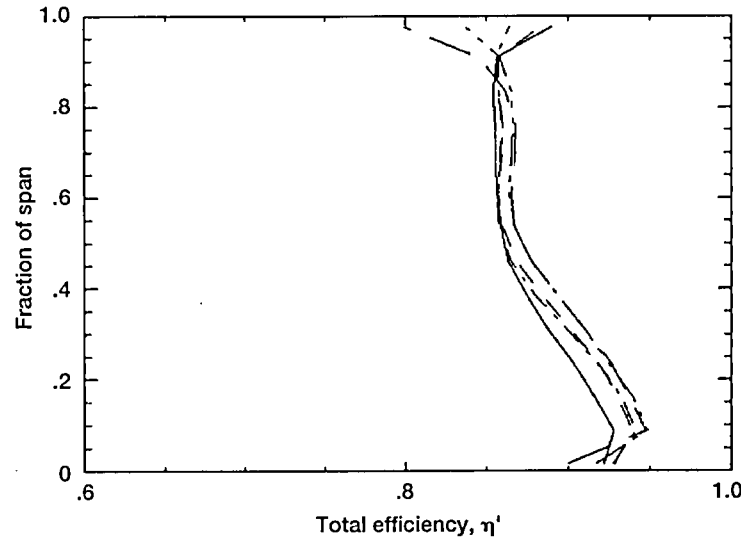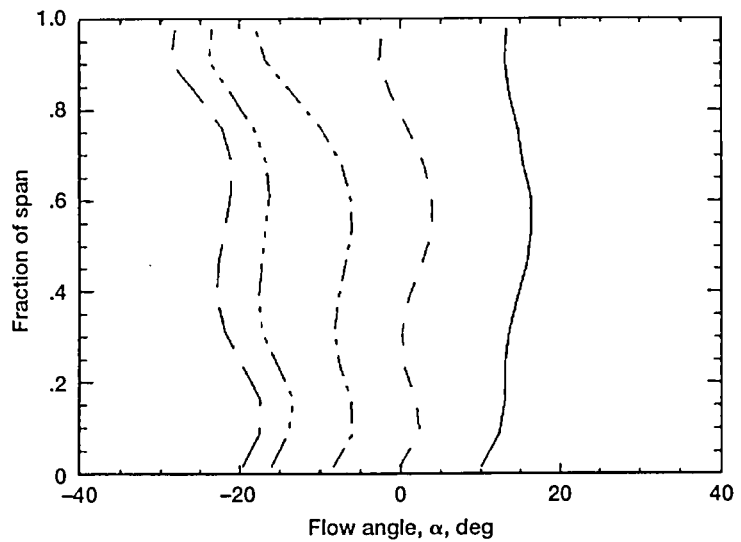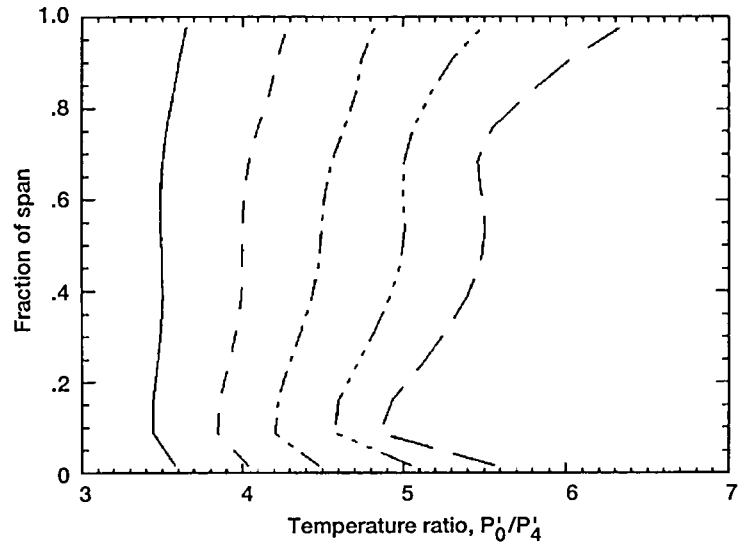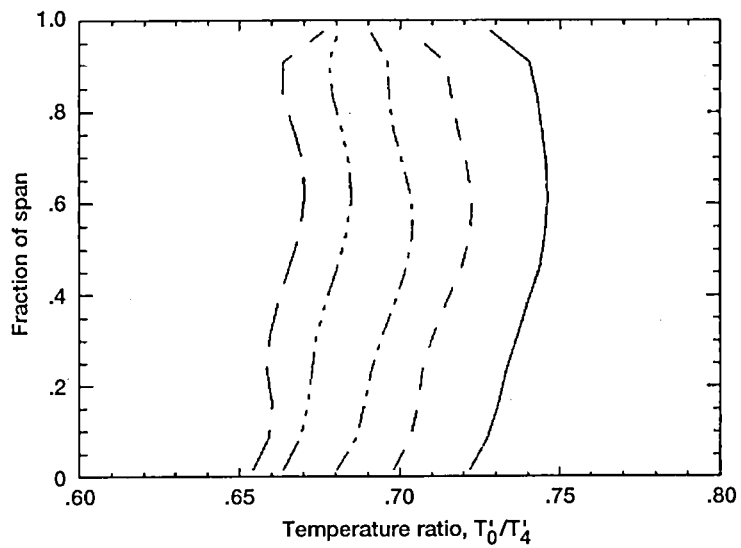
Figure 42.—Turbine exit radial surveys at 110 percent of design speed for rotor I-stator II configuration at various pressure ratios.
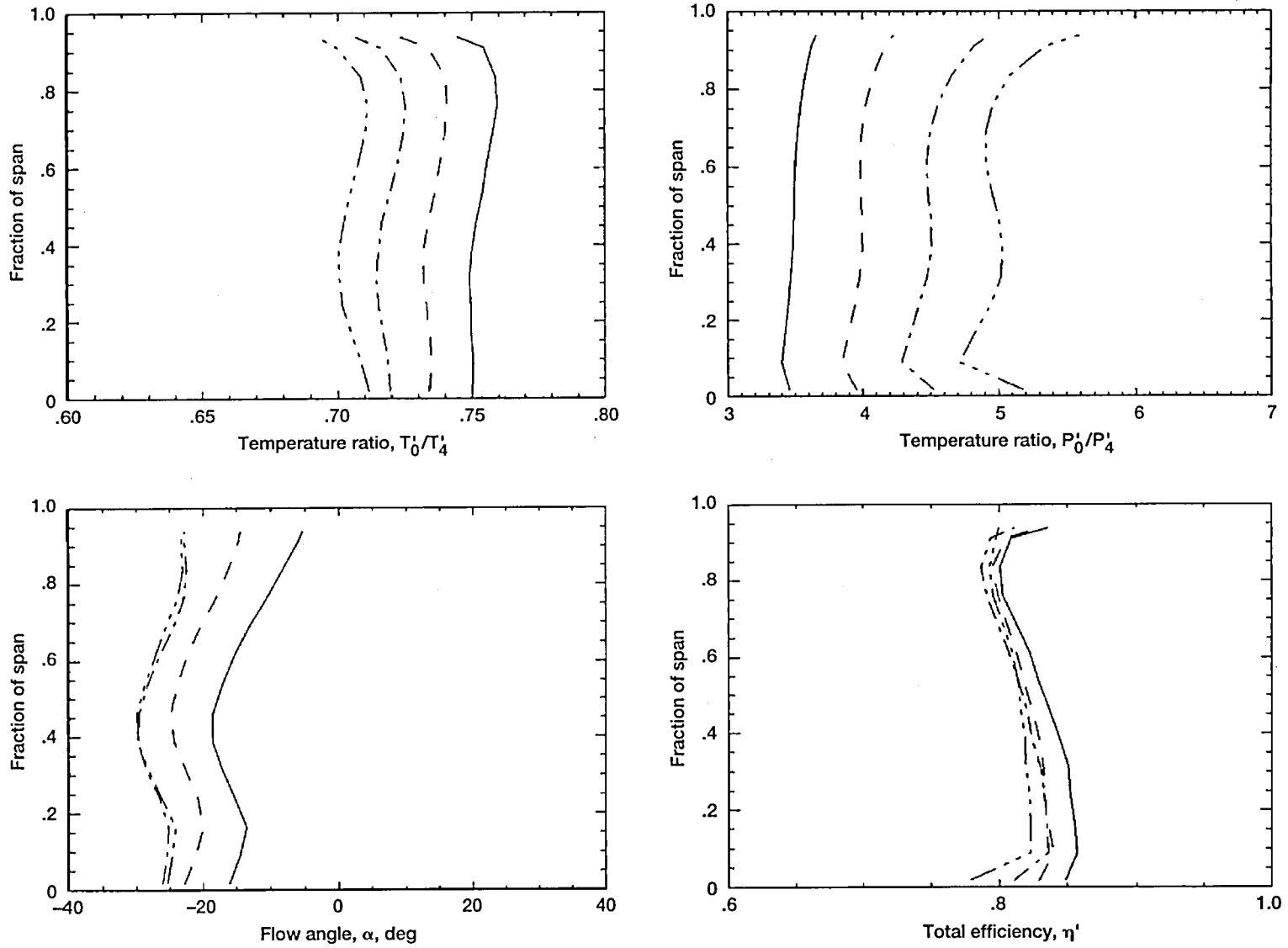
Figure 43.—Turbine exit radial surveys at 80 percent of design speed for rotor II-stator II configuration at various pressure ratios.
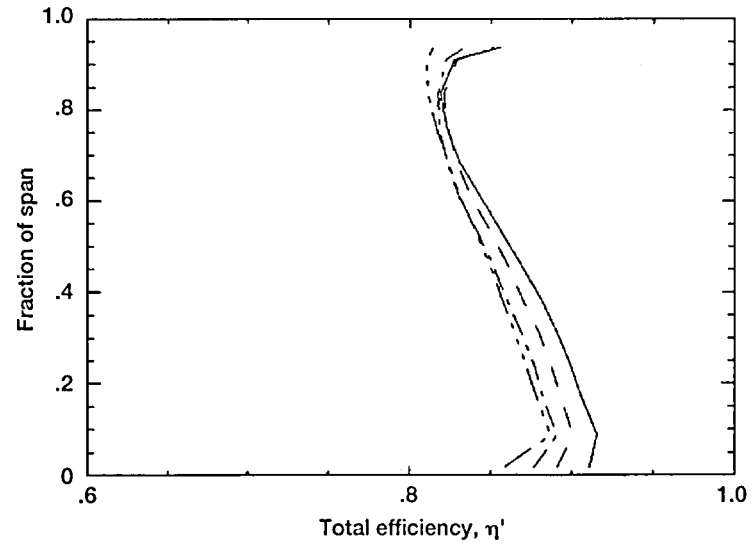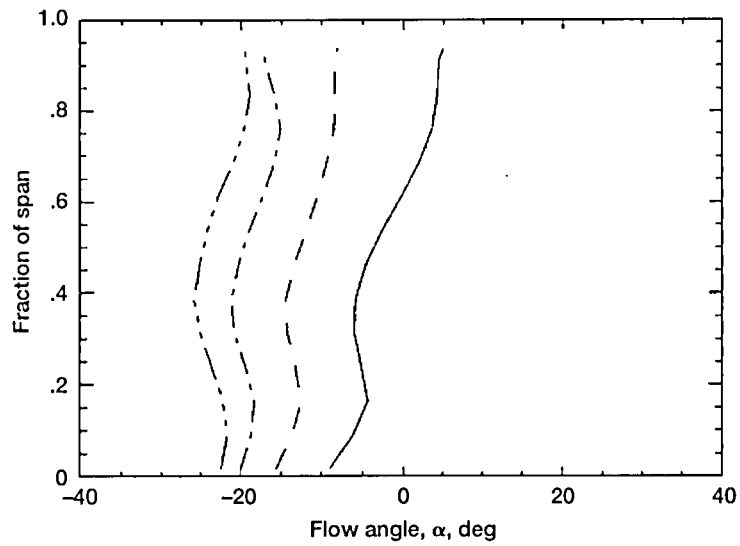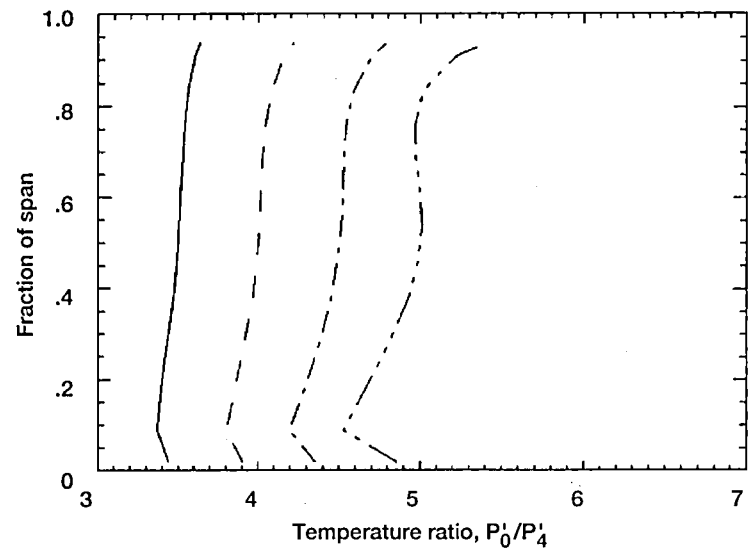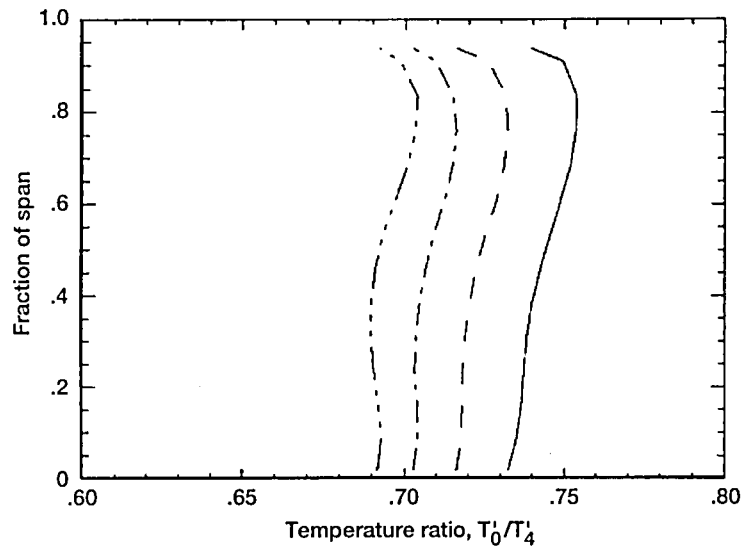
Figure 44.—Turbine exit radial surveys at 90 percent of design speed for rotor II-stator II configuration at various pressure ratios.
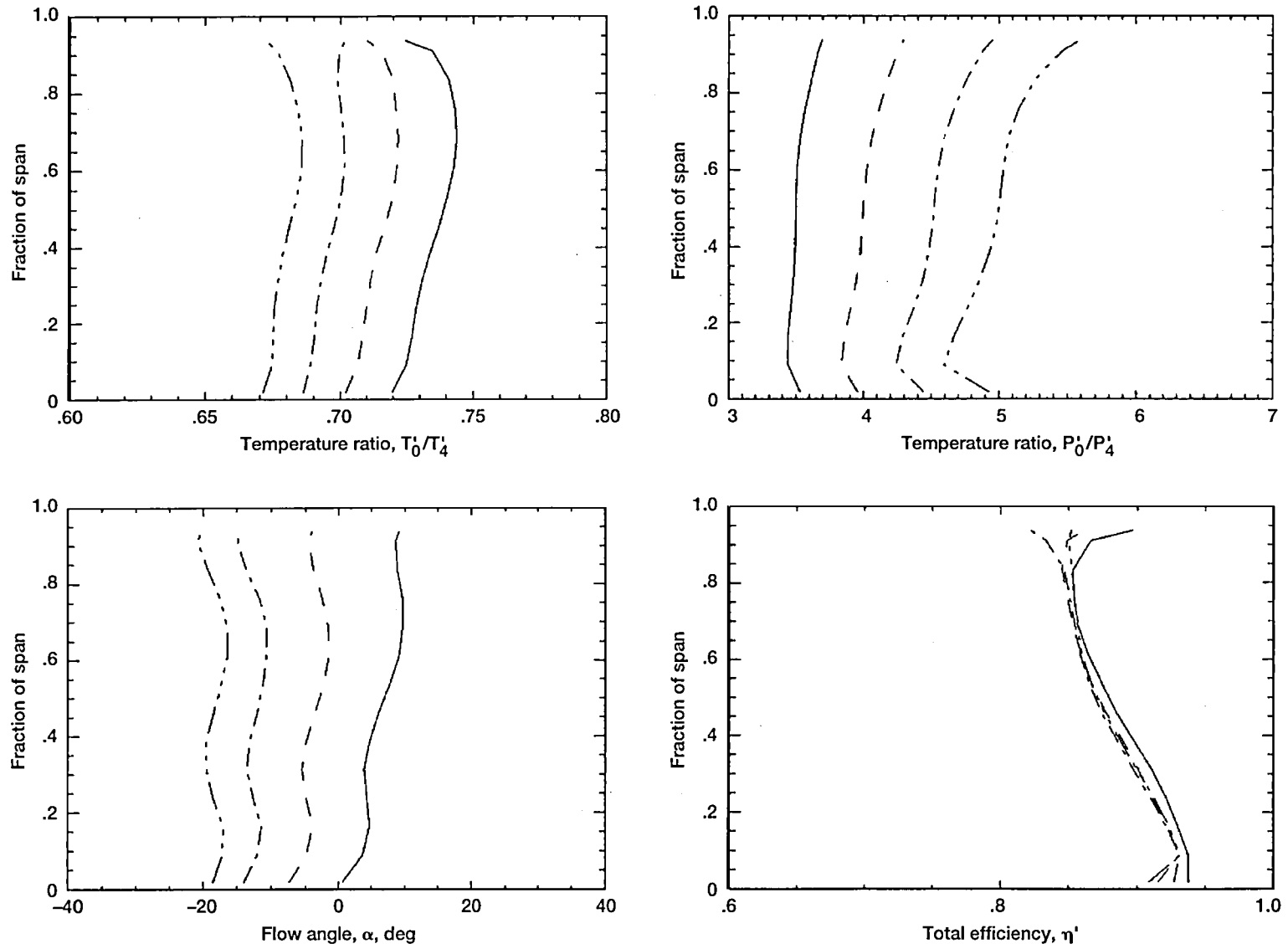
Figure 45.—Turbine exit radial surveys at 100 percent of design speed for rotor II-stator II configuration at various pressure ratios.
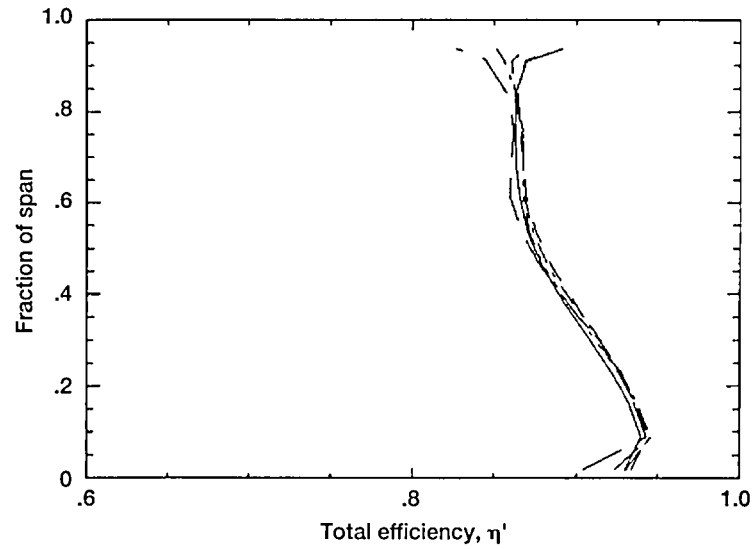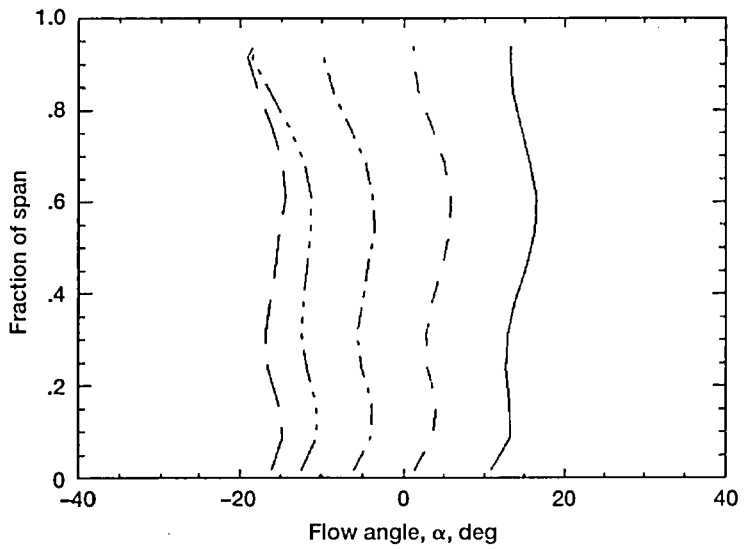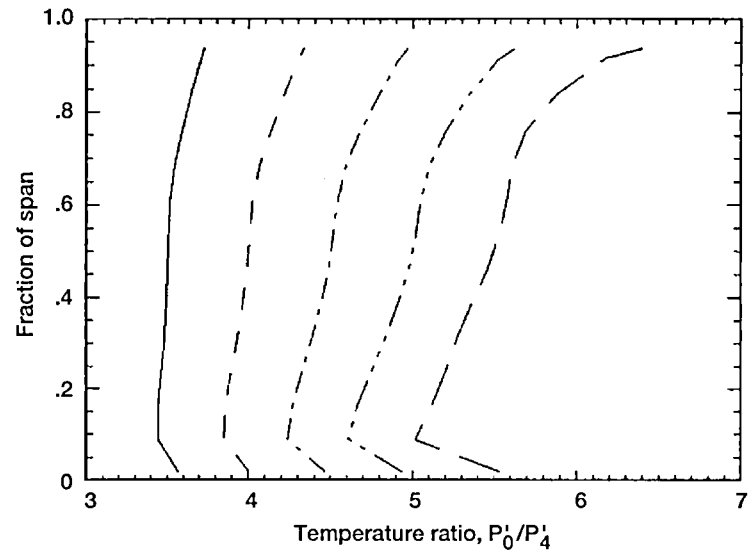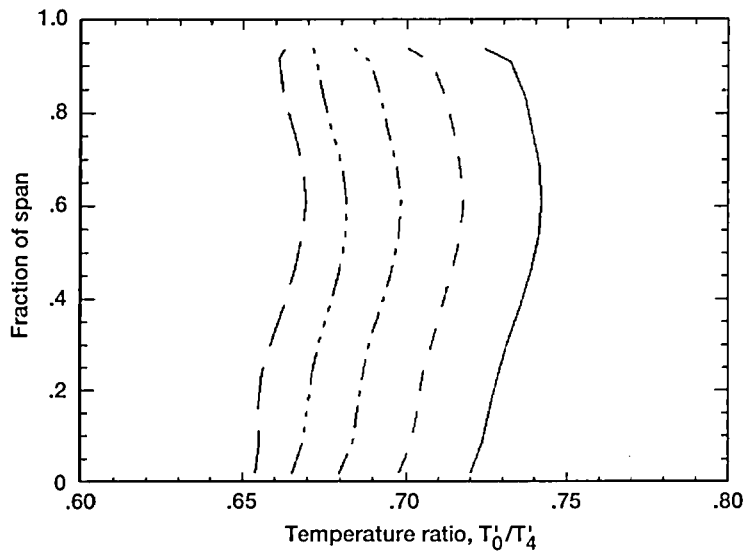
Figure 46.—Turbine exit radial surveys at 110 percent of design speed for rotor II-stator II configuration at various pressure ratios.
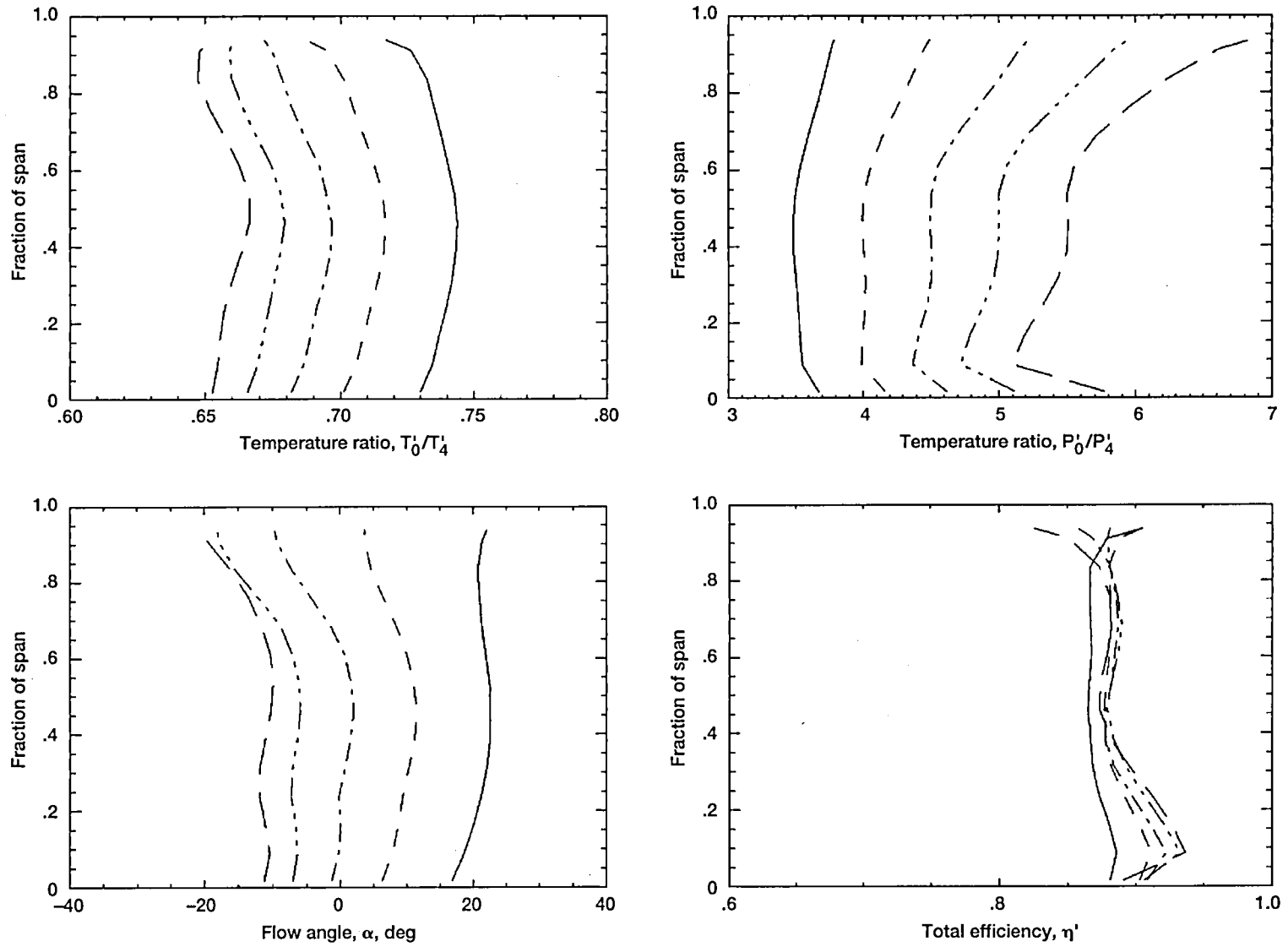
Figure 47.—Turbine exit radial surveys at 120 percent of design speed for rotor II-stator II configuration at various pressure ratios.

Appendix C

Shroud Static Pressure Port Locations

Hardware	Measurement station	Percent of rotor chord
Inlet	0	−46.4
Stator inlet	1	−28.6
Stator exit	2	−6.0
Rotor leading edge		0
		12.0
		22.0
		32.0
		42.0
		49.0
		54.0
		63.0
		67.0
		77.0
Rotor trailing edge		94.0
Rotor exit		101.0
		104.0
		109.0
		114.0
		119.0
		123.0
		128.0
		132.0
		137.0
		143.0
		147.0
Rotor exit survey location	3	160.7
Exit rake location	4	210.7

References

1. Huber, F.W.; and Ni, R.R.: Application of a Multi-Stage 3D Euler Solver to the Design of Turbines for Advanced Propulsion Systems. AIAA Paper 89–2578, July 1989.
2. Fredmonski, A.J. et al.: Design and Experimental Evaluation of Compact Radial-Inflow Turbine. AIAA Paper 91–2127, June 1991.
3. Simonyi, P.S.; and Boyle, R.J: Comparison of a Quasi-3D Analysis and Experimental Performance for Three Compact Radial Turbine. AIAA Paper 91–2128, June 1991.
4. Heidmann, J.D.: A Three-Dimensional Navier-Stokes Stage Analysis of the Flow Through a Compact Radial Turbine. AIAA Paper 2564, June 1991.
5. Tirres, L.: A Comparison of the Calculated and Experimental Off-Design Performance of a Radial Flow Turbine. NASA CR–189207, 1991
6. Nowlin, B.C.; and Verhoff, V.G.: Small Engine Components Test Facility Turbine Testing Cell. NASA TM–00887, 1988.
7. Rogo, C.: Cooled Variable Nozzle Radial Turbine for Rotor-Craft Applications. NASA CR–165397, 1981.
8. Rogo, C.: Variable Area Radial Turbine Fabrication and Test Program. NASA CR–175091, 1986.
9. Kofskey, M.G.; and Nusbaum, W.J.: Cold Performance Evaluation of 4.97-inch Radial-Inflow Turbine Design for Single-Shaft Brayton Cycle Space Power System. NASA TN D–5090, 1969.
10. Holeski, D.E.; and Kofskey, M.G.: Cold Performance Evaluation of a 6.02–in. Radial-Inflow Turbine Designed for a 10-Kilowatt Shaft Output Brayton Cycle Space Power Generator System. NASA TN D–2987, 1965.
11. Futral, S.M., Jr.; and Wasserbauer, C.A.: Experimental Performance Evaluation of a 4.59-Inch Radial-Inflow Turbine With and Without Splitter Blades. NASA TN D–7015, 1971.
12. McLallin, K.L.; and Haas, J.E.: Experimental Performance and Analysis of 15.04-Centimeter Tip Diameter, Radial-Inflow Turbine With Work Factor of 1.126 and Thick Blading. NASA TP–1730, 1980.
13. Kofskey, M.G.; and Wasserbauer, C.A.: Experimental Evaluation of a 3.50-Inch Radial Turbine Designed for a 10-Kilowatt Space Power System. NASA TN D–5550, 1969.

REPORT DOCUMENTATION PAGE

1. AGENCY USE ONLY (Leave blank)	2. REPORT DATE	3. REPORT TYPE AND DATES COVERED
	July 1995	Technical Paper

4. TITLE AND SUBTITLE

Aerodynamic Evaluation of Two Compact Radial-Inflow Turbine Rotors

6. AUTHOR(S)

P. Susan Simonyi, Richard J. Roelke, Roy G. Stabe, Brentley C. Nowlin, and Danielle DiCicco

5. FUNDING NUMBERS

WU–505–62–10

7. PERFORMING ORGANIZATION NAME(S) AND ADDRESS(ES)

National Aeronautics and Space Administration
Lewis Research Center
Cleveland, Ohio 44135–3191

8. PERFORMING ORGANIZATION REPORT NUMBER

E–9213

9. SPONSORING/MONITORING AGENCY NAME(S) AND ADDRESS(ES)

National Aeronautics and Space Administration
Washington, D.C. 20546–0001

10. SPONSORING/MONITORING AGENCY REPORT NUMBER

NASA TP–3514

12a. DISTRIBUTION/AVAILABILITY STATEMENT

Unclassified - Unlimited
Subject Category 37

12b. DISTRIBUTION CODE

13. ABSTRACT (Maximum 200 words)

The aerodynamic evaluation of two highly loaded compact radial turbine rotors was conducted at the NASA Lewis Research Center Small Engine Component Test Facility (SECTF). The experimental results were used for proof-of-concept, for modeling radial inflow turbine rotors, and for providing data for code verification. Two rotors were designed to have a shorter axial length, up to a 10-percent reduced diameter, a lighter weight, and equal or higher efficiencies compared with those of conventional radial inflow turbine rotors. Three configurations were tested: rotor I, having a 40-percent shorter axial length, with the design stator (stator I); rotor I with the design stator vanes closed down (stator II); and rotor II, slightly shorter axially and having higher loading, with stator II. The stator had 36 vanes and the rotors each had 14 solid blades. Although presently uncooled, the rotor blades were designed for thicknesses which would allow cooling passages to be added. The overall stage performance measurements and the rotor and stator exit flow field surveys were obtained. Measurements of steady state temperatures, pressures, mass flow rates, flow angles, and output power were made at various operating conditions. Data were obtained at corrected speeds of 80, 90, 100, 110, and 120 percent of design over a range of equivalent inlet-to-exit pressure ratios of 3.5, 4.0, 4.5, and 5.0, the maximum pressure ratio achieved. The test showed that the configuration of rotor I with stator I running at the design pressure ratio produced a flow rate which was 5.6 percent higher than expected. This result indicated the need to close down the stator flow area to reduce the flow. The flow area reduction was accomplished by restaggering the vanes. Rotor I was retested with the closed-down stator vanes and achieved the correct mass flow. Rotor II was tested only with the restaggered vanes. The test results of the three turbine configurations were nearly identical. Although the measured efficiencies of the compact designs fell 2 to 3 points below the predicted efficiency of 91 percent, they did meet and exceed by up to 2.5 percentage points the efficiencies of state-of-the-art turbines found in the literature.

14. SUBJECT TERMS

Compact radial turbine; Experiment; Performance

15. NUMBER OF PAGES

71

16. PRICE CODE

A04

17. SECURITY CLASSIFICATION OF REPORT	18. SECURITY CLASSIFICATION OF THIS PAGE	19. SECURITY CLASSIFICATION OF ABSTRACT	20. LIMITATION OF ABSTRACT
Unclassified	Unclassified	Unclassified	

National Aeronautics and
Space Administration

Lewis Research Center
21000 Brookpark Rd.
Cleveland, OH 44135-3191